JEM Journal of Experimental Medicine

ARTICLE

Repression of the B cell identity factor Pax5 is not required for plasma cell development

Grace J. Liu[1], Markus Jaritz[1], Miriam Wöhner[1], Benedikt Agerer[2], Andreas Bergthaler[2], Stephen G. Malin[1], and Meinrad Busslinger[1]

B cell and plasma cell fates are controlled by different transcriptional networks, as exemplified by the mutually exclusive expression and cross-antagonism of the B cell identity factor Pax5 and the plasma cell regulator Blimp1. It has been postulated that repression of *Pax5* by Blimp1 is essential for plasma cell development. Here, we challenged this hypothesis by analyzing the *Igh*$^{Pax5/+}$ mouse, which expressed a *Pax5* minigene from the immunoglobulin heavy-chain locus. Despite high Pax5 expression, plasma cells efficiently developed in young *Igh*$^{Pax5/+}$ mice at steady state and upon immunization, while their number moderately declined in older mice. Although Pax5 significantly deregulated the plasma cell expression program, key plasma cell regulators were normally expressed in *Igh*$^{Pax5/+}$ plasma cells. While IgM and IgA secretion by *Igh*$^{Pax5/+}$ plasma cells was normal, IgG secretion was modestly decreased. Hence, *Pax5* repression is not essential for robust plasma cell development and antibody secretion, although it is required for optimal IgG production and accumulation of long-lived plasma cells.

Introduction

Plasma cells provide acute and long-term protection of the host against infection through secretion of high-affinity antibodies that recognize an almost unlimited number of pathogens (Nutt et al., 2015). The highly diverse B cell antigen receptor (BCR) repertoire is generated in early B cell development by V(D)J recombination of the immunoglobulin heavy-chain (*Igh*) and light-chain (*Igk* or *Igl*) gene loci (Alt et al., 2013). Somatic hypermutation of the rearranged *Ig* genes subsequently creates pathogen-specific high-affinity BCRs in germinal center (GC) B cells (Victora and Nussenzweig, 2012). The terminal differentiation of B cells to antibody-secreting plasma cells is characterized by a massive reprogramming of gene expression (Minnich et al., 2016; Shi et al., 2015). While the transcription factors Irf4, Blimp1, E2A, and E2-2 are required for the development of plasma cells (Gloury et al., 2016; Minnich et al., 2016; Nutt et al., 2015; Tellier et al., 2016; Wöhner et al., 2016), the unfolded protein response regulator Xbp1 is essential for controlling the enormous expansion of the ER and thus the high capacity of antibody secretion in plasma cells (Reimold et al., 2001; Shaffer et al., 2004). In contrast, the development, function, and identity of B cells is regulated by a different transcriptional network, including the B cell–specific regulators Pax5 and Ebf1 (Boller and Grosschedl, 2014; Medvedovic et al., 2011).

The transcription factor Pax5 controls the commitment of lymphoid progenitors to the B cell pathway at the onset of B-lymphopoiesis (Medvedovic et al., 2011; Nutt et al., 1999). Pax5 fulfills its B cell commitment function by repressing lineage-inappropriate genes to suppress alternative lineage fates and by activating B-lymphoid–specific genes to promote B cell development (Delogu et al., 2006; Nutt et al., 1999; Revilla-I-Domingo et al., 2012; Schebesta et al., 2007). Pax5 functions as a B cell identity factor throughout B cell development, as mature splenic B cells upon conditional Pax5 loss are able to dedifferentiate to uncommitted progenitors in the bone marrow, which can further develop into functional T cells (Cobaleda et al., 2007). In late B lymphopoiesis, Pax5 is required for the generation or survival of all mature B cell types, as it controls signaling from both the BCR and Toll-like receptors (unpublished data). In addition, PAX5 functions as a haploinsufficient tumor suppressor in one third of all human B-progenitor acute lymphoblastic leukemias (Gu et al., 2019), while it acts as an oncoprotein in a subset of B cell non-Hodgkin's lymphomas carrying an *IGH-PAX5* translocation (Medvedovic et al., 2013).

The transcriptional regulators Pax5 and Blimp1 (encoded by the *Prdm1* gene) are expressed in a mutually exclusive manner in the B cell lineages. Pax5 is expressed at all stages of B cell development from the pro–B cell to the activated B cell stage and,

[1]Research Institute of Molecular Pathology, Vienna BioCenter, Vienna, Austria; [2]Research Center for Molecular Medicine of the Austrian Academy of Sciences, Vienna, Austria.

Correspondence to Meinrad Busslinger: meinrad.busslinger@imp.ac.at; S.G. Malin's present address is Center for Molecular Medicine, Department of Medicine, Karolinska Institutet, and Karolinska University Hospital, Stockholm, Sweden.

upon terminal differentiation, is repressed in plasmablasts and plasma cells (Fuxa and Busslinger, 2007). In contrast, Blimp1 expression is not detected in B cells, but is initiated in pre-plasmablasts and maintained in all antibody-secreting cells (ASCs) in peripheral lymphoid organs and in long-lived plasma cells in the bone marrow (Kallies et al., 2004). Consistent with their mutually exclusive expression patterns, Pax5 and Blimp1 cross-antagonize each other and their respective gene expression programs, as Pax5 directly represses the *Prdm1* (Blimp1) gene in mature B cells (Delogu et al., 2006; Revilla-I-Domingo et al., 2012), while Blimp1 directly represses *Pax5* in plasmablasts and plasma cells (Minnich et al., 2016).

Deletion of the endogenous *Pax5* gene in the chicken DT40 B cell line leads to plasmacytic differentiation at the expense of the B cell phenotype, as Blimp1 and Xbp1 expression is induced together with increased IgM secretion, while Bcl6 and Ebf1 expression is repressed (Nera et al., 2006). Ectopic expression of Pax5 was furthermore shown to suppress the spontaneous differentiation of a mature B cell line to ASCs (Usui et al., 1997). Moreover, retroviral expression of Pax5 in splenic B cells was shown to prevent lipopolysaccharide-induced differentiation to IgM-secreting plasmablasts (Lin et al., 2002). Together, this evidence led to the commonly held view that the repression of *Pax5* is essential for plasma cell differentiation to occur (Nutt et al., 2015). However, this hypothesis has never been experimentally challenged in an in vivo mouse model.

We have previously generated a mouse model for a human *IGH-PAX5* translocation (Busslinger et al., 1996) by inserting a *PAX5* minigene into the endogenous *Igh* locus adjacent to the Eμ enhancer (Souabni et al., 2007; Fig. S1 A). Heterozygous $Igh^{P5ki/+}$ mice in the absence of a cooperating oncogenic mutation do not give rise to B cell lymphoma and only rarely develop T-lymphoblastic lymphoma after a long latency (Souabni et al., 2007). In wild-type mice, the expression of the rearranged *Igh* mRNA is known to increase 30-fold during the transition from activated B cells to plasmablasts, while the *Pax5* gene is simultaneously repressed (Minnich et al., 2016). In contrast, the plasmablasts and plasma cells of $Igh^{P5ki/+}$ mice should continue to express Pax5 from the *Pax5* minigene due to the increased transcriptional activity of the *Igh* locus, while the endogenous *Pax5* gene is repressed by Blimp1. Using this mouse model, we have now demonstrated that, despite extensive gene expression changes, plasmablasts and plasma cells efficiently developed in the presence of continued Pax5 expression. The Pax5-expressing plasma cells were functional as they secreted antigen-specific antibodies in response to immunization, although the longevity of plasma cells in the bone marrow was moderately decreased with time. Contrary to the current dogma, these data therefore demonstrate that the repression of Pax5 is not required for plasma cell development to occur.

Results

B and T cells are present at normal frequencies in $Igh^{Pax5/+}$ mice

As plasmablasts and plasma cells are defined by their expression of Blimp1 (*Prdm1*), we used the $Prdm1^{Gfp}$ reporter allele (Kallies et al., 2004) for identifying these rare cells by flow cytometry. For this purpose, we first deleted the *frt*-flanked IRES-Gfp reporter gene located downstream of the *PAX5* minigene in the Igh^{P5ki} allele (Souabni et al., 2007) by Flpe-mediated recombination to generate the Igh^{Pax5} allele (Fig. S1 A). We subsequently performed all analyses with experimental $Igh^{Pax5/+}$ $Prdm1^{Gfp/+}$ and control $Igh^{+/+}$ $Prdm1^{Gfp/+}$ mice. For simplicity, we will abbreviate the two genotypes to $Igh^{Pax5/+}$ and $Igh^{+/+}$, except for experiments where GFP expression from the $Prdm1^{Gfp}$ allele was essential for plasma cell identification. Since the *Igh* locus is known to be already active in lymphoid progenitors of $Igh^{P5ki/+}$ mice (Souabni et al., 2007), we examined B cell development in the bone marrow as well as B and T cells in the spleen and lymph nodes of experimental and control mice by flow cytometry. B cell development was normal in the bone marrow of $Igh^{Pax5/+}$ mice compared with control mice, except for a twofold increase in pro-B cells (Fig. 1 A), which is likely caused by the precocious expression of Pax5 in the preceding lymphoid progenitors (Souabni et al., 2007). Similarly, the follicular and marginal zone B cells were present at comparable frequencies in the spleen of $Igh^{Pax5/+}$ and control littermates (Fig. 1 B). The $CD8^+$ T cells were also unaffected in the lymph nodes of $Igh^{Pax5/+}$ mice, while a small reduction in $CD4^+$ T cells was observed in these mice compared with control littermates (Fig. 1 C).

Analysis of Pax5 expression by intracellular flow cytometry revealed that the Pax5 protein levels were similar or only slightly increased in the different B cell populations of $Igh^{Pax5/+}$ mice compared with control littermates (Fig. 1, D and E), consistent with the absence of a B cell phenotype. Both $CD4^+$ and $CD8^+$ T cells in the lymph nodes of $Igh^{Pax5/+}$ mice showed ectopic and variegated Pax5 expression (Fig. 1 F), in agreement with the fact that the *Igh* locus is transcriptionally active in T cells (Kemp et al., 1980). Hence, Pax5 expression levels were minimally increased in B cells and moderately elevated in T cells, consistent with normal B and T cell development in $Igh^{Pax5/+}$ mice.

Efficient plasma cell development in the presence of Pax5 expression

To determine whether ectopic Pax5 expression can inhibit plasma cell differentiation, naive B cells from $Igh^{Pax5/+}$ $Prdm1^{Gfp/+}$ mice were stimulated in vitro with bacterial LPS. After 4 d of stimulation, $Igh^{Pax5/+}$ $Prdm1^{Gfp/+}$ plasmablasts could be readily detected as GFP^+CD138^+ cells and were only minimally decreased in frequency compared with control $Igh^{+/+}$ $Prdm1^{Gfp/+}$ plasmablasts (Fig. 2 A). As expected, the $Igh^{Pax5/+}$ plasmablasts expressed strongly elevated levels of Pax5 protein, as shown by intracellular Pax5 staining (Fig. 2 B). Detailed analysis revealed a rapid and progressive loss of Pax5 protein expression during the differentiation of activated $Igh^{+/+}$ B cells to plasmablasts (Fig. S1, B and C). In contrast, Pax5 protein expression was only moderately reduced during the transition from activated $Igh^{Pax5/+}$ B cells to plasmablasts, which was likely caused by repression of the endogenous *Pax5* gene (Fig. S1 C). Ectopic transcription from the Igh^{Pax5} allele instead gave rise to the high Pax5 protein expression observed in $Igh^{Pax5/+}$ plasmablasts (Fig. S1 C). Together, these data indicate that, contrary to expectation, ectopic Pax5

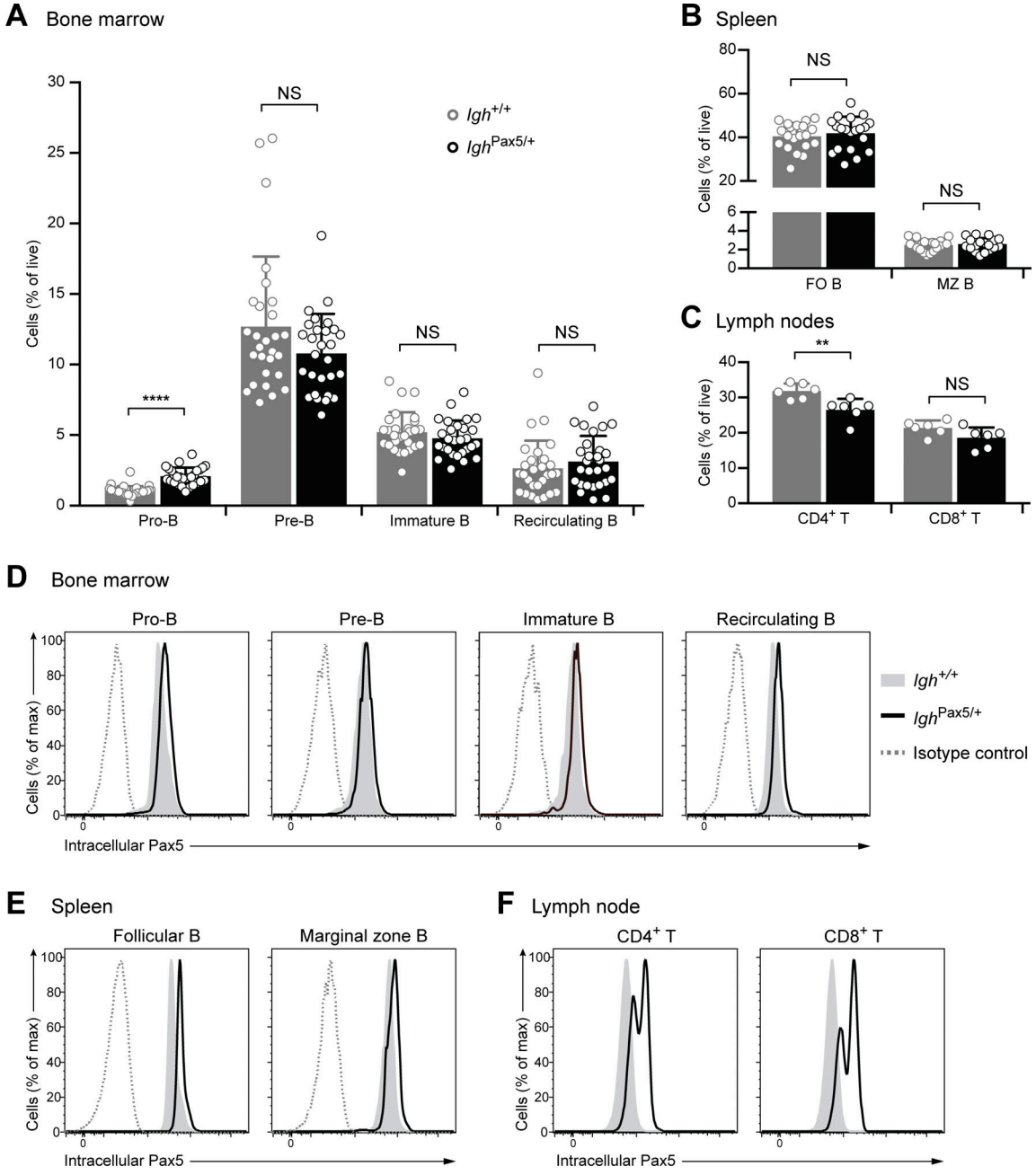

Figure 1. **Normal B cell development in $Igh^{Pax5/+}$ mice. (A–C)** Flow-cytometric analysis of bone marrow (A), spleen (B), and lymph node (C) cells from 8–12-wk-old $Igh^{Pax5/+}$ (black) and $Igh^{+/+}$ (gray) littermates. The relative frequency was determined for pro-B ($CD19^+Kit^+CD2^-IgM^-$), pre-B ($CD19^+Kit^-CD2^+IgM^-$), immature B ($CD19^+IgM^+IgD^-$), and recirculating B ($CD19^+IgM^{lo}IgD^{hi}$) cells in the bone marrow (A), follicular ($CD19^+CD21^{lo}CD23^{hi}$), and marginal zone ($CD19^+CD21^{hi}CD23^{lo}$) B cells in the spleen (B) and mature $CD4^+$ and $CD8^+$ T cells in the lymph nodes (C). The flow-cytometric data were obtained in seven (A), five (B), or two (C) independent experiments. Statistical data (A–C) are shown as mean values with SD and were analyzed by the two-tailed unpaired Student's *t* test; **, $P < 0.01$; ****, $P < 0.0001$. NS, not significant ($P > 0.05$). Each dot corresponds to one mouse. **(D–F)** Flow-cytometric analysis of Pax5 expression by intracellular staining of developing and recirculating B cells in the bone marrow (D), mature B cells in the spleen (E), and mature T cells in the lymph nodes of $Igh^{Pax5/+}$ (black line) and $Igh^{+/+}$ (gray filled) littermates. The specificity of the anti-Pax5 antibody (IgG2a) was controlled by staining of the different B cell types with a control IgG2a isotype antibody (gray dashed line).

expression from the *Igh* locus did not prevent in vitro plasmablast differentiation.

We next interrogated the ability of $Igh^{Pax5/+}$ $Prdm1^{Gfp/+}$ mice to generate plasma cells in response to an antigen challenge in vivo. 14 d after immunization with the T cell–dependent antigen 4-hydroxy-3-nitrophenylacetyl (NP)–conjugated keyhole limpet hemocyanin (NP-KLH; in alum), GFP^+CD138^+ plasma cells were detected in the spleens of $Igh^{Pax5/+}$ $Prdm1^{Gfp/+}$ mice at similar frequencies as in control $Igh^{+/+}$ $Prdm1^{Gfp/+}$ mice (Fig. 2 C). As the $Prdm1^{Gfp}$ reporter allele can distinguish between less mature GFP^{int} and mature GFP^{hi} plasma cells (Kallies et al., 2004), closer analysis of the GFP expression level within the

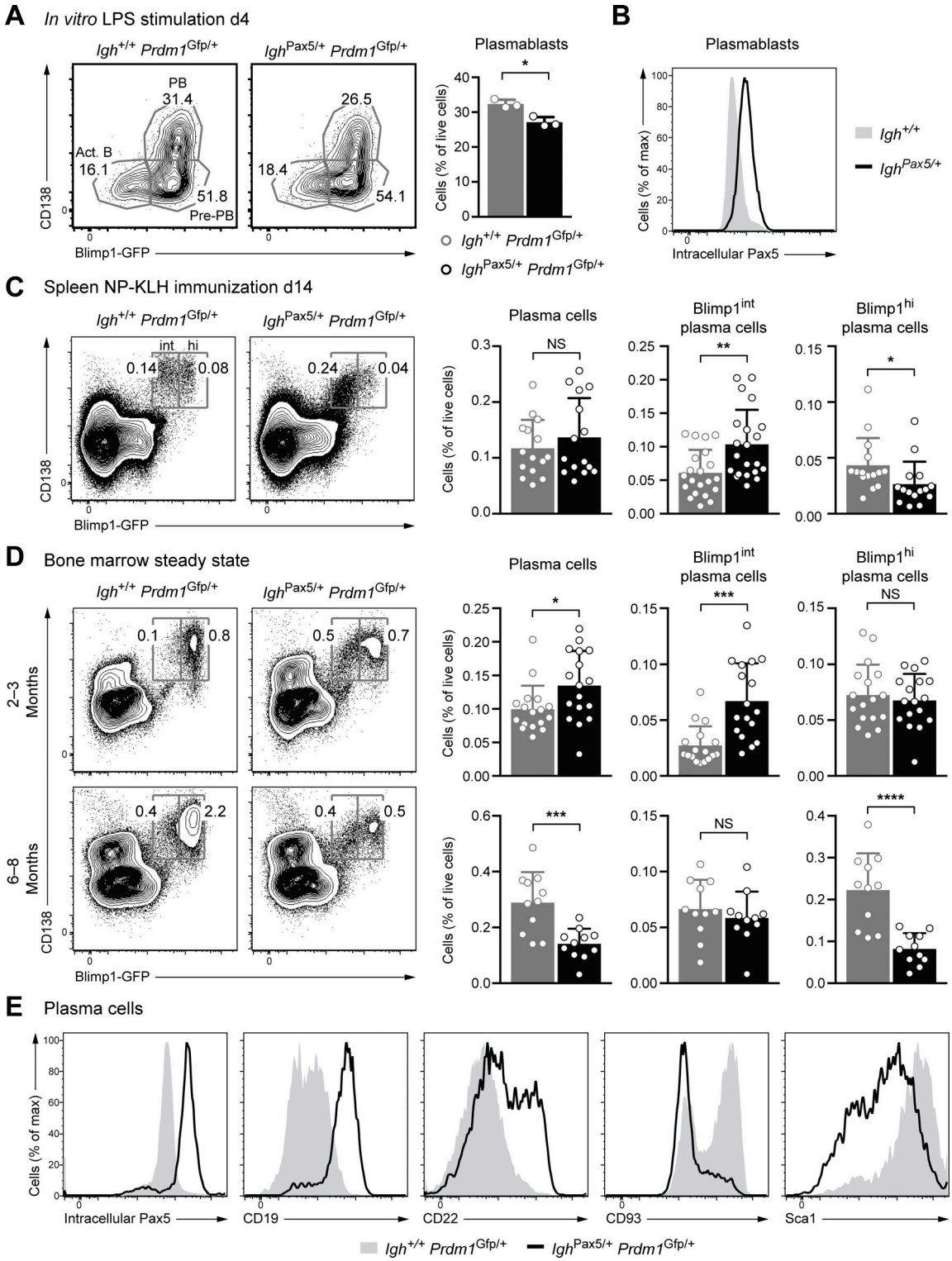

Figure 2. **Plasma cell differentiation in the presence of ectopic Pax5 expression. (A)** Flow-cytometric analysis and frequencies of activated B cells (GFP^-CD138^-), pre-plasmablasts (GFP^+CD138^-), and plasmablasts (GFP^+CD138^+) at day 4 after LPS stimulation of naive B cells isolated from $Igh^{Pax5/+}$ $Prdm1^{Gfp/+}$ (black) and $Igh^{+/+}$ $Prdm1^{Gfp/+}$ (gray) mice. Percentages of cells in each gate are indicated. The data are representative of three independent experiments. **(B)** Flow-cytometric analysis of Pax5 expression by intracellular staining of $Igh^{Pax5/+}$ (black line) and $Igh^{+/+}$ (gray filled) plasmablasts after 4 d of LPS stimulation (see also Fig. S1, B and C). **(C)** Flow-cytometric analysis of plasma cells ($Lin^-B220^{int}CD138^+GFP^+$) in the spleen of $Igh^{Pax5/+}$ $Prdm1^{Gfp/+}$ (black) and $Igh^{+/+}$ $Prdm1^{Gfp/+}$ (gray) littermates 14 d after immunization with NP-KLH (in alum). The plasma cells were pregated on $Lin^-(CD4^-CD8^-CD21^-CD49b^-)B220^{int}$ cells and were divided into less mature (GFP^{int}) and mature (GFP^{hi}) plasma cells. Frequencies of total, GFP^{int}, and GFP^{hi} plasma cells are indicated on the right. The data are pooled from four independent experiments. **(D)** Flow-cytometric analysis of plasma cells ($Lin^-B220^{int}CD138^+GFP^+$) from the bone marrow of nonimmunized $Igh^{+/+}$ $Prdm1^{Gfp/+}$ and $Igh^{Pax5/+}$ $Prdm1^{Gfp/+}$ littermates at the age of 2–3 mo (top row) or 6–8 mo (bottom row). The frequencies of total, GFP^{int},

and GFP^{hi} plasma cells are summarized on the right. The data are pooled from five (2–3 mo) or three (6–8 mo) independent experiments. Statistical data (A, C, and D) are shown as mean values with SD and were analyzed by the two-tailed unpaired Student's *t* test; *, P < 0.05; **, P < 0.01; ***, P < 0.001; ****, P < 0.0001. NS, not significant (P > 0.05). Each dot (A, C, and D) corresponds to one mouse. **(E)** Flow-cytometric analysis of intracellular Pax5 expression and cell surface expression of CD19, CD22, CD93, and Sca1 on total plasma cells from the bone marrow of *Igh*$^{Pax5/+}$ *Prdm1*$^{Gfp/+}$ (black line) and *Igh*$^{+/+}$ *Prdm1*$^{Gfp/+}$ (gray filled) mice. Data are representative of three experiments.

bulk GFP$^+$CD138$^+$ plasma cell population revealed a moderate skewing of the plasma cells in *Igh*$^{Pax5/+}$ *Prdm1*$^{Gfp/+}$ mice toward the less mature GFP^{int} phenotype in contrast to the control *Igh*$^{+/+}$ *Prdm1*$^{Gfp/+}$ mice (Fig. 2 C).

In addition to investigating plasma cells generated in secondary lymphoid organs following an antigen challenge, we also examined the long-lived plasma cells that accumulate in the bone marrow at steady state. In young mice at the age of 2–3 mo, plasma cells (GFP$^+$CD138$^+$) were present in *Igh*$^{Pax5/+}$ *Prdm1*$^{Gfp/+}$ mice at a slightly elevated frequency compared with control *Igh*$^{+/+}$ *Prdm1*$^{Gfp/+}$ mice (Fig. 2 D, top row). This increase in *Igh*$^{Pax5/+}$ *Prdm1*$^{Gfp/+}$ mice was due to an increase of less mature GFP^{int} plasma cells, while the mature GFP^{hi} plasma cells were present at a similar frequency in experimental and control mice (Fig. 2 D, top row). In contrast, fewer total plasma cells were detected in the bone marrow of older *Igh*$^{Pax5/+}$ *Prdm1*$^{Gfp/+}$ mice relative to control mice at the age of 6–8 mo (Fig. 2 D, bottom row). While the less mature GFP^{int} plasma cells were present at similar frequency, older *Igh*$^{Pax5/+}$ *Prdm1*$^{Gfp/+}$ mice failed to accumulate mature GFP^{hi} plasma cells to the same extent as their control *Igh*$^{+/+}$ *Prdm1*$^{Gfp/+}$ littermates (Fig. 2 D, bottom row). In summary, ectopic Pax5 expression is compatible with robust plasma cell development, but subsequently interferes with long-term accumulation of mature plasma cells in the bone marrow.

Using intracellular flow cytometry, we confirmed that *Igh*$^{Pax5/+}$ *Prdm1*$^{Gfp/+}$ plasma cells expressed greatly elevated levels of Pax5 protein (Fig. 2 E). Flow-cytometric analyses furthermore revealed increased expression of the cell surface proteins CD19 and CD22 as well as decreased expression of CD93 and Sca1 on plasma cells of *Igh*$^{Pax5/+}$ *Prdm1*$^{Gfp/+}$ mice compared with control *Igh*$^{+/+}$ *Prdm1*$^{Gfp/+}$ littermates (Fig. 2 E). Importantly, *Cd19* and *Cd22* are known activated Pax5 target genes in pro-B cells, while *Sca1* and *Cd93* are repressed Pax5 target gene identified in pro-B and mature B cells, respectively (Revilla-I-Domingo et al., 2012). Together, these observations demonstrated that the ectopically expressed Pax5 protein was transcriptionally active in *Igh*$^{Pax5/+}$ *Prdm1*$^{Gfp/+}$ plasma cells.

Pax5-dependent deregulation of the plasma cell gene expression program

To systematically analyze the effect of Pax5 on gene expression in plasma cells, we first investigated the genome-wide Pax5-binding pattern in *Igh*$^{Pax5/+}$ and control *Igh*$^{+/+}$ plasmablasts, which were isolated at day 4 of LPS stimulation to a purity of 92–95% by immunomagnetic enrichment with CD138-MicroBeads (Fig. S2 A). In parallel, we analyzed the CD138-depleted cell fractions, which were strongly enriched for activated B cells (73–75%; Fig. S2 A) and were therefore referred to as "activated B cells." As we expected minimal Pax5 binding in *Igh*$^{+/+}$ plasmablasts, we performed calibrated chromatin immunoprecipitation coupled with deep sequencing (ChIP-seq) experiments (Hu et al., 2015) to verify the quality of the ChIP-seq data obtained with these cells. For this, we mixed chromatin prepared from the purified mouse plasmablasts or activated B cells with chromatin from chicken DT40 B cells at a 9:1 ratio before ChIP-seq analysis with an antibody that recognized the conserved paired domain of mouse and chicken Pax5 (see Materials and methods). Peak calling with a stringent P value of $<10^{-10}$ identified 17,907 and 9,934 Pax5 peaks in activated *Igh*$^{Pax5/+}$ and *Igh*$^{+/+}$ B cells, respectively, which were characterized by a similar average peak height (read density; Fig. 3, A and B; and Fig. S2, B and C). Notably, 20,481 Pax5 peaks of a high read density were identified in *Igh*$^{Pax5/+}$ plasmablasts. In contrast, only 1,618 Pax5 peaks, characterized by a low read density, could be determined in *Igh*$^{+/+}$ plasmablasts (Fig. 3, A and B; and Fig. S2, B and C), indicating that only residual Pax5 was still bound to chromatin upon loss of Pax5 expression in wild-type plasmablasts (Fig. 2 B and Fig. S1 C). Pax5 binding at the genes *Cd19*, *Cd22*, *Cd79a*, and *Id3*, all of which have previously been identified as activated Pax5 target genes in pro-B cells (Revilla-I-Domingo et al., 2012; Schebesta et al., 2007), exemplified how Pax5 peaks are maintained in *Igh*$^{Pax5/+}$ plasmablasts and are lost in control *Igh*$^{+/+}$ plasmablasts (Fig. 3 C). Hence, these data demonstrate efficient binding of Pax5 across the genome in plasmablasts that normally do not express this transcription factor.

We next investigated the degree to which the ectopically expressed Pax5 protein could interfere with the transcriptional program of plasmablasts and plasma cells in *Igh*$^{Pax5/+}$ *Prdm1*$^{Gfp/+}$ mice compared with control *Igh*$^{+/+}$ *Prdm1*$^{Gfp/+}$ mice. For this, we performed RNA-sequencing (RNA-seq) analysis with sorted in vitro LPS-differentiated plasmablasts (CD22$^-$CD138$^+$GFP$^+$) or plasma cells (CD138$^+$GFP$^+$), which were purified ex vivo from the bone marrow of 6–8-mo-old mice by immunomagnetic enrichment with CD138-MicroBeads before flow-cytometric isolation (Fig. S3 A). As the mature GFP^{hi} plasma cells expressed higher levels of CD138 compared with the less mature GFP^{int} plasma cells in the bone marrow of *Igh*$^{Pax5/+}$ *Prdm1*$^{Gfp/+}$ mice (Fig. 2 D), the immunomagnetic enrichment of CD138$^+$ cells efficiently selected for mature GFP^{hi} plasma cells (Fig. S3 A). By comparing the gene expression changes between *Igh*$^{Pax5/+}$ and control *Igh*$^{+/+}$ plasmablasts, we identified 122 Pax5-activated and 78 Pax5-repressed genes, based on an expression difference of more than twofold, an adjusted P value of <0.05, and an expression value of >5 TPM (transcripts per million) in one of the two plasmablast cell types (Fig. S3 B and Table S1). By using a higher threefold cutoff, we identified 246 Pax5-activated and 66 Pax5-repressed genes in *Igh*$^{Pax5/+}$ plasma cells compared with control *Igh*$^{+/+}$ plasma cells (Fig. 4 A and Table S2), which resulted in an overlap of 62 activated and 14 repressed genes between in vitro differentiated plasmablasts and long-term plasma cells

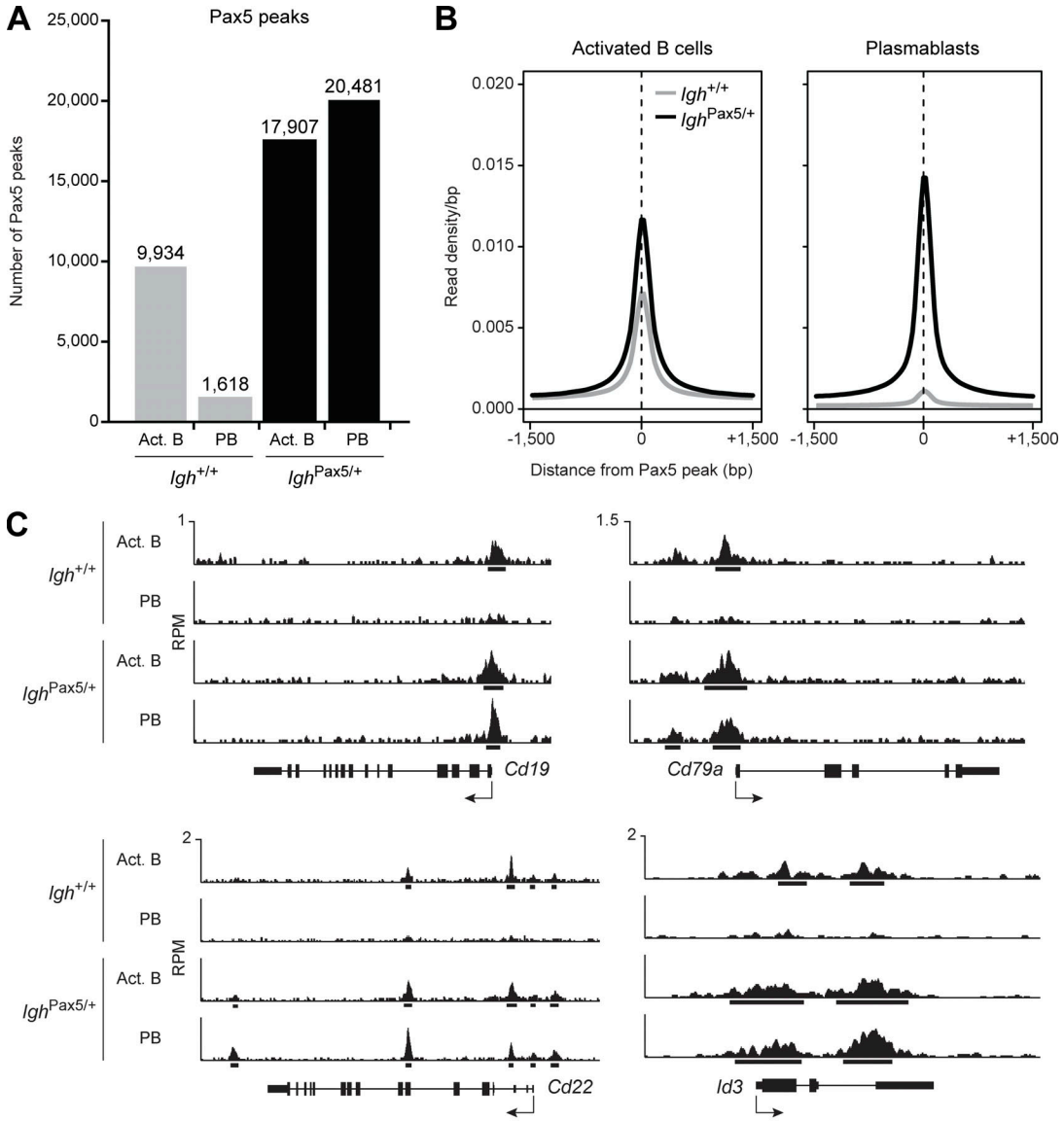

Figure 3. **Efficient Pax5 binding across the genome of $Igh^{Pax5/+}$ plasmablasts. (A)** ChIP-seq analysis of Pax5 binding in activated B cells and plasmablasts that were isolated by magnetic cell sorting (see Fig. S2 A) at day 4 after LPS stimulation of $Igh^{Pax5/+}$ (black) and $Igh^{+/+}$ (gray) B cells. The indicated number of Pax5 peaks in each cell type was identified by stringent MACS peak calling with a P value of $<10^{-10}$. **(B)** Densities of Pax5 binding. Average read density profiles aligned at the center of the Pax5 peak are shown for activated B cells (left) and plasmablasts (right) of the $Igh^{Pax5/+}$ (black line) or $Igh^{+/+}$ (gray line) genotype. **(C)** Binding of Pax5 at the indicated genes in $Igh^{+/+}$ and $Igh^{Pax5/+}$ activated B cells and plasmablasts. Horizontal bars below the ChIP-seq tracks indicate binding regions identified by MACS peak calling. The exon-intron structures are shown below. The reads per million (RPM) values of Pax5 binding in the murine cells were normalized according to genome-wide Pax5 binding detected in the chicken DT40 spike-in cells within each sample used for calibrated ChIP-seq analysis (see Materials and methods). Act. B., activated B cells; PB, plasmablast.

(Fig. S3 C). Annotation of the Pax5-regulated genes identified in $Igh^{Pax5/+}$ plasma cells revealed that a large fraction of the activated and repressed genes code for cell surface proteins, signal transducers, and metabolic enzymes, which could potentially affect the function of Pax5-expressing plasma cells (Fig. 4 B). Pax5 binding, determined in $Igh^{Pax5/+}$ plasmablasts (Fig. 3), was observed at 190 (77%) of the 246 Pax5-activated genes and only at 28 (42%) of the 66 Pax5-repressed genes (Table S2), suggesting that Pax5 may be more effective in directly activating genes in $Igh^{Pax5/+}$ plasma cells. Consistent with this finding, 67 of the 246 Pax5-activated genes in $Igh^{Pax5/+}$ plasma cells were previously identified as activated Pax5 target genes, while only 8 of the 66 Pax5-repressed genes were earlier described as repressed Pax5 target genes in pro-B and mature B cells (Delogu et al., 2006; Revilla-I-Domingo et al., 2012; Schebesta et al., 2007; Table S2).

Gene set enrichment analysis (GSEA) revealed that genes up-regulated during normal plasmablast or plasma cell development (Minnich et al., 2016) were significantly enriched as Pax5-repressed genes, while conversely genes down-regulated during terminal differentiation were enriched as Pax5-activated genes in $Igh^{Pax5/+}$ plasmablasts and $Igh^{Pax5/+}$ plasma cells, respectively

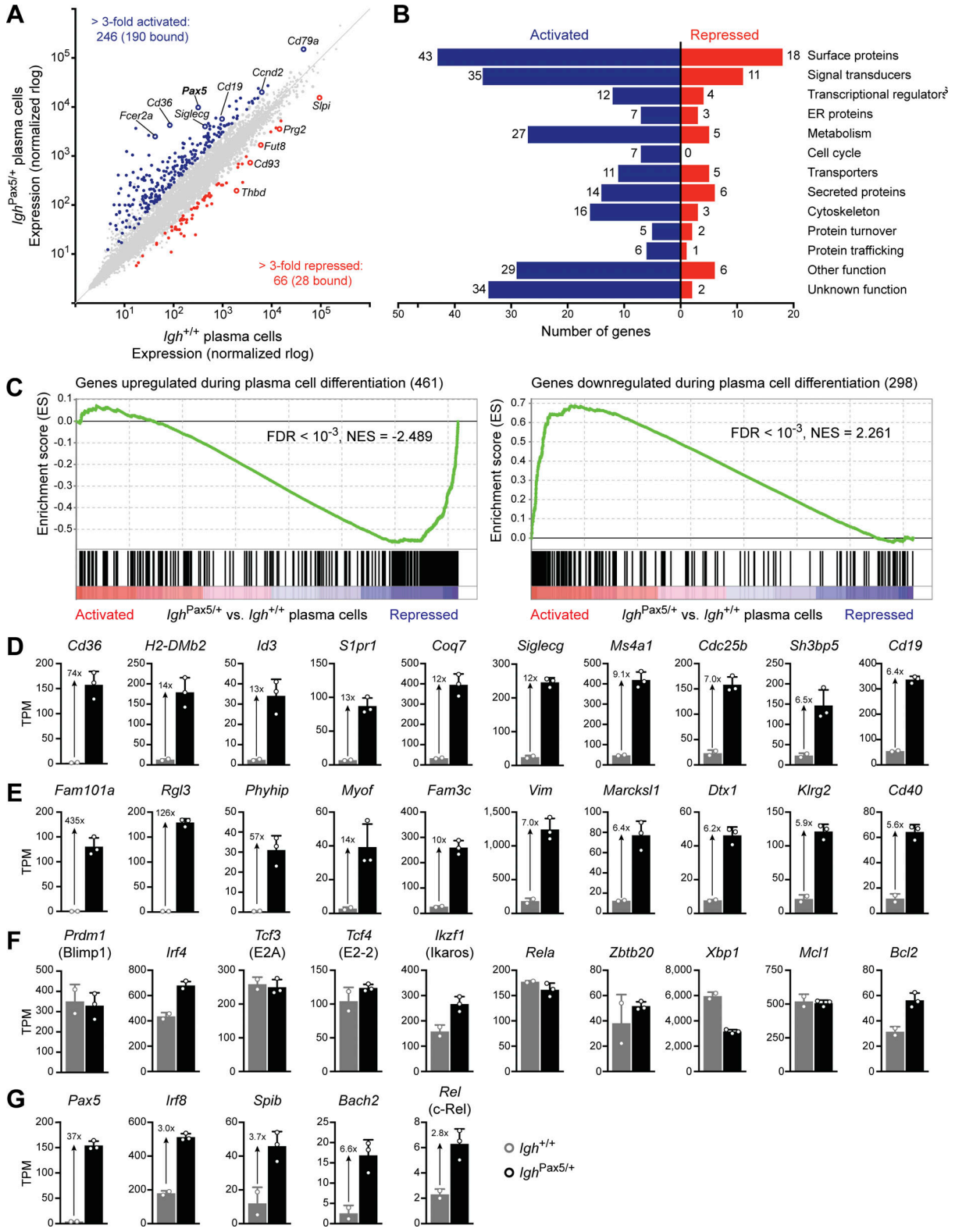

Figure 4. **Pax5-dependent deregulation of the plasma cell gene expression program. (A)** Scatter plot of gene expression differences between *Igh*$^{Pax5/+}$ and *Igh*$^{+/+}$ plasma cells that were isolated from the bone marrow of 6–8-mo-old mice, as described in Fig. S3 A, before RNA-sequencing. The expression data of individual genes (indicated by dots) are plotted as normalized rlog (regularized logarithm) values. Genes with an expression difference of greater than threefold, an adjusted P value of <0.05, and a TPM value of >5 (in at least one sample) are colored in blue or red, corresponding to activation or repression by Pax5. The reference gene *Pax5* (in bold) and 11 genes previously identified as activated or repressed Pax5 target genes in pro-B or mature B cells (Revilla-I-Domingo et al., 2012) are highlighted by open circles. **(B)** Functional classification and quantification (number) of proteins encoded by Pax5-activated and Pax5-repressed target genes identified in A. **(C)** GSEA of 461 up-regulated genes (left) or 298 down-regulated genes (right) during the B cell–to–plasma cell transition, as

compared with the ranked log_2-fold expression changes in $Igh^{Pax5/+}$ versus $Igh^{+/+}$ plasma cells. The 461 and 298 genes were previously identified as being up-regulated or down-regulated >10-fold between mature B cells and bone marrow plasma cells, respectively (Minnich et al., 2016). NES, normalized enrichment score; FDR, false discovery rate. **(D–G)** Expression of selected genes in $Igh^{Pax5/+}$ (black) and $Igh^{+/+}$ (gray) plasma cells. The expression data are shown as mean TPM values with SD and are based on two ($Igh^{+/+}$) and three ($Igh^{Pax5/+}$) independent RNA-seq experiments. Each dot represents one experiment performed with pooled plasma cells from 5–10 mice per genotype. **(D)** Pax5-bound and -activated genes in $Igh^{Pax5/+}$ plasma cells that have previously been identified as activated Pax5 target genes in pro-B cells or mature B cells (Revilla-I-Domingo et al., 2012; Schebesta et al., 2007). **(E)** Pax5-bound and -activated genes in $Igh^{Pax5/+}$ plasma cells that have not been identified as Pax5-regulated genes in developing B cells. **(F)** Key regulatory genes with known functions in the development, function, or survival of plasma cells. **(G)** Genes coding for transcriptional repressors that prevent Blimp1 expression and the plasma cell fate in mature B cells. All five genes were bound by Pax5 in $Igh^{Pax5/+}$ plasmablasts.

(Fig. 4 C and Fig. S3 D). The expression of selected genes, which qualified as activated Pax5 target genes both in $Igh^{Pax5/+}$ plasma cells and pro-B or mature B cells, are shown in Fig. 4 D, while the expression of genes that were identified as activated Pax5 target genes only in $Igh^{Pax5/+}$ plasma cells is shown in Fig. 4 E. Likewise, the expression of common and plasma cell–specific repressed Pax5 target genes is indicated in Fig. S3, E and F. Despite the substantial gene expression changes, the key plasma cell regulators Blimp1, Irf4, E2A, E2-2, Ikaros, RelA, and Zbtb20 (Chevrier et al., 2014; Nutt et al., 2015; Roy et al., 2019) were expressed at similar or slightly elevated levels in $Igh^{Pax5/+}$ plasma cells relative to $Igh^{+/+}$ plasma cells (Fig. 4 F), which explains why plasma cells could efficiently develop in $Igh^{Pax5/+}$ mice. The twofold decreased expression of *Xbp1* in $Igh^{Pax5/+}$ plasma cells mimics the heterozygous *Xbp1* condition, which was reported not to affect antibody secretion in $Xbp1^{+/-}$ plasmablasts (Taubenheim et al., 2012). Notably, Blimp1 was normally expressed in $Igh^{Pax5/+}$ plasma cells despite the fact that Pax5 activated the expression of Irf8, SpiB (*Spib*), Bach2, and c-Rel (*Rel*; Fig. 4 G), which have also been implicated as repressors of the *Prdm1* gene in mature B cells (Carotta et al., 2014; Ochiai et al., 2006; Roy et al., 2019; Willis et al., 2017). Importantly, the expression of the pro-survival genes *Mcl1* and *Bcl2* was similar or twofold increased in $Igh^{Pax5/+}$ plasma cells compared with $Igh^{+/+}$ plasma cells (Fig. 4 F). Finally, the expression of genes, which code for cell adhesion proteins and surface receptors involved in the control of plasma cell homing and survival (Nutt et al., 2015), was 1.6-fold increased (*Cxcr4*) or 1.3-fold to 2.4-fold decreased (*Tnfrsf17* [BCMA], *Cd44*, *Il6ra*, *Cd28*, and *Itga4* [VLA4]) in $Igh^{Pax5/+}$ plasma cells relative to control cells (Fig. S3 G). More importantly, the mRNA expression of the cell surface lectin CD93, implicated in plasma cell persistence (Chevrier et al., 2009), was 5.3-fold repressed by ectopic Pax5 expression in plasma cells (Fig. 2 E and Fig. S3 E), suggesting that the loss of CD93, possibly in combination with the minimally reduced expression of other cell surface receptors, may contribute to the impaired longevity of $Igh^{Pax5/+}$ plasma cells in older mice.

Normal IgM secretion by Pax5-expressing plasma cells

Given the Pax5-dependent deregulation of gene expression in plasma cells, we next investigated whether the plasma cells of $Igh^{Pax5/+}$ mice were functional, particularly with regard to antibody secretion. To this end, we performed ELISPOT assays to determine the number and secretory capacity of IgM and IgG ASCs. The secretory capacity was determined by the size of the ELISPOT, which correlates with the amount of antibody secretion by individual plasma cells. Under steady-state conditions, the number and ELISPOT size of IgM-producing ASCs were similar in the bone marrow of young $Igh^{Pax5/+}$ and control $Igh^{+/+}$ mice at the age of 2–3 mo (Fig. 5 A), indicating that the Pax5-expressing plasma cells retained the ability to undergo the transcriptional and morphological changes required for immunoglobulin secretion. However, the number and ELISPOT size of IgG-producing ASCs were reduced in $Igh^{Pax5/+}$ mice (Fig. 5 A). Similar results were obtained with mice at the age of 6–8 mo, except for the observed 2.2-fold decrease in the number of IgM-producing ASCs in the bone marrow of $Igh^{Pax5/+}$ mice compared with control littermates (Fig. 5 B). This reduction likely reflects the twofold decrease in total plasma cell numbers that we observed by flow-cytometric analysis in old $Igh^{Pax5/+}$ mice (Fig. 2 D, bottom row). Moreover, ELISA measurements of the serum titers of the different Ig isotypes in young and old mice revealed a moderate decrease only for IgG1 in $Igh^{Pax5/+}$ mice (Fig. S4, A and B), in agreement with the corresponding reduction of the ELISPOT size of IgG ASCs in these mice (Fig. 5, A and B).

To interrogate the capacity of ectopic Pax5-expressing plasma cells to mount a specific antibody response to a defined T cell–dependent antigen, we immunized $Igh^{Pax5/+}$ and control mice with NP-KLH (in alum) and performed ELISPOT assays at day 14 after immunization to detect NP-specific plasma cells. NP-specific IgM ASCs were present at similar numbers and had a similar ELISPOT size in both the spleen and bone marrow of $Igh^{Pax5/+}$ and control mice (Fig. 5, C and D). However, as observed already under steady-state conditions, both the number and ELISPOT size (secretion) of the NP-specific IgG1 ASCs were reduced in the spleens and bone marrow of immunized $Igh^{Pax5/+}$ mice compared with control mice (Fig. 5, C and D). Together, these data indicate that IgM-specific plasma cells were generated in normal numbers and secreted similar amounts of IgM in $Igh^{Pax5/+}$ mice in contrast to the IgG-specific plasma cells, which were present at lower numbers and showed a moderate defect in IgG secretion.

To gain further insight into the IgG-specific plasma cell phenotype, we compared the expression of *Igh* mRNAs of different Ig isotypes by interrogating the RNA-seq data of $Igh^{Pax5/+}$ and control $Igh^{+/+}$ plasma cells (Fig. 4 A). Notably, the *Ighm* and *Igha* mRNAs were present at similar abundance in plasma cells of both genotypes, whereas the expression of *Ighg1*, *Ighg2c*, and *Ighg3* mRNA was reduced in $Igh^{Pax5/+}$ plasma cells compared with control plasma cells (Fig. S4 C). These data strongly suggest that the IgG-specific plasma cells were generated in lower numbers due to a defect in class switch recombination (CSR) to IgG isotypes in $Igh^{Pax5/+}$ B cells.

Finally, we used transition electron microscopy to analyze the morphology of the plasma cells isolated from the bone marrow of 6–8-mo-old $Igh^{Pax5/+}$ and control $Igh^{+/+}$ mice. The

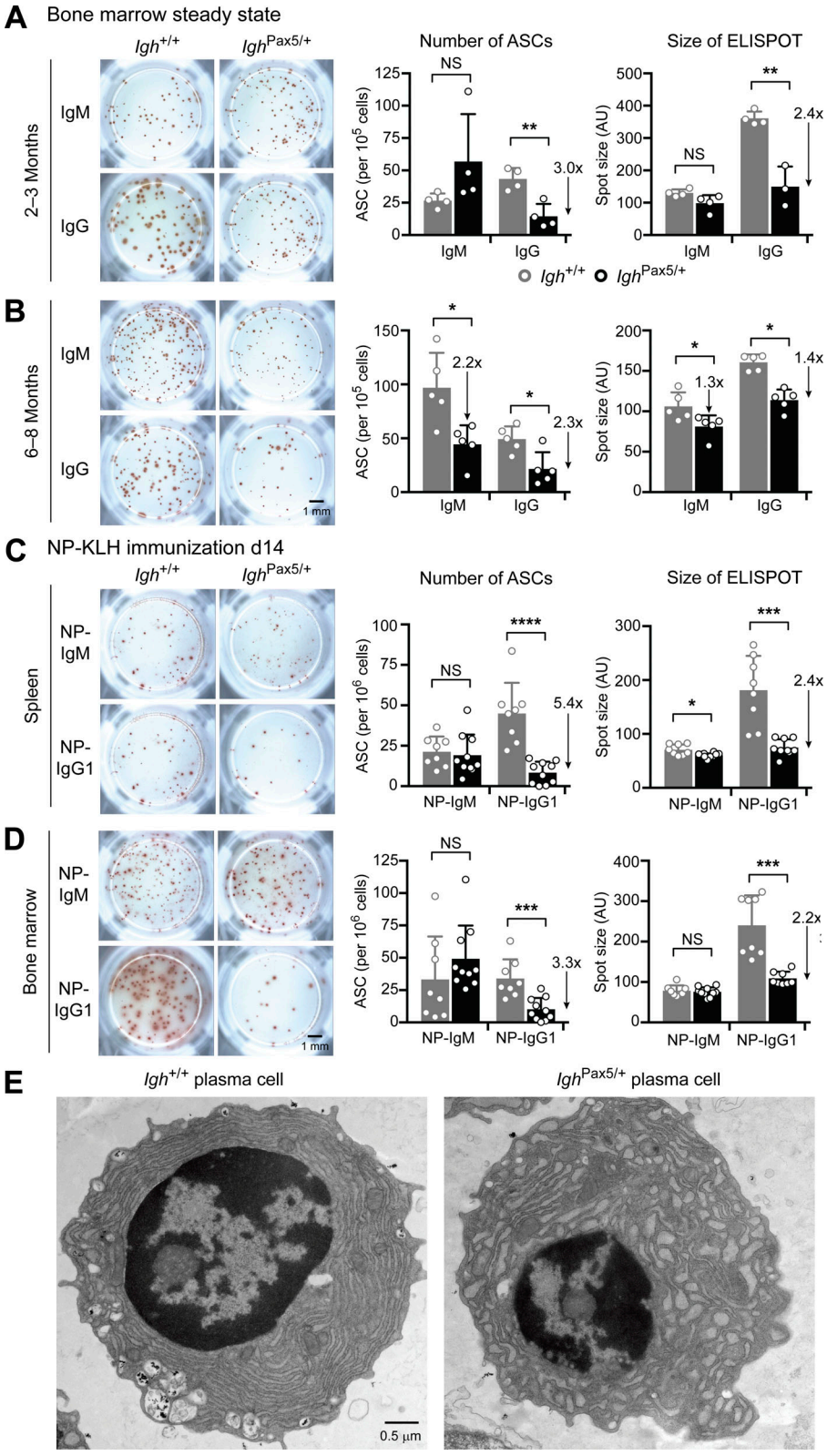

Figure 5. **Antibody secretion by *Igh*$^{Pax5/+}$ plasma cells. (A and B)** Antibody secretion by *Igh*$^{Pax5/+}$ and *Igh*$^{+/+}$ plasma cells under steady-state conditions. The numbers of IgM and IgG ASCs in the bone marrow of *Igh*$^{Pax5/+}$ (black) and *Igh*$^{+/+}$ (gray) mice at the age of 2–3 mo (A) and 6–8 mo (B) were determined by ELISPOT assay by incubating RBC-depleted bone marrow cells (2×10^5) on IgM- or IgG-coated plates for 6 h before determination of the number and size of the ELISPOTs. Images of representative ELISPOT wells (left), the mean cell number (middle), and the median ELISPOT size (right) are shown for IgM and IgG ASCs. **(C and D)** Antibody secretion by *Igh*$^{Pax5/+}$ and *Igh*$^{+/+}$ plasma cells 14 d after immunization with NP-KLH (in alum). The numbers of anti–NP-IgM or anti–NP-IgG1 ASCs in the spleen (C) and bone marrow (D) were determined by ELISPOT assay by incubating RBC-depleted cells (2×10^6) from the spleen or bone marrow on NP_{20}-BSA-coated plates before the determination of the number and size of the ELISPOTs. Images of representative ELISPOT wells (left), the mean cell number (middle), and the median ELISPOT size (right) are shown for anti–NP-IgM and anti–NP-IgG1 ASCs. The data (C and D) are pooled from two independent immunization experiments. Statistical data (A–D) are shown as mean values with SD and were analyzed by the two-tailed unpaired Student's *t* test; *, $P < 0.05$; **, $P < 0.01$; ***, $P < 0.001$; ****, $P < 0.0001$. NS, not significant ($P > 0.05$). Each dot (A–D) corresponds to one mouse. **(E)** Electron microscope images of plasma cells isolated from the bone marrow of *Igh*$^{Pax5/+}$ and *Igh*$^{+/+}$ mice at the age of 6–8 mo. 1 representative image of 10 individual plasma cells analyzed per genotype is shown. The length of the indicated scale bars is 1 mm (B and D) or 0.5 µm (E).

ultrastructure of the Pax5-expressing plasma cells was mostly normal compared with that of control plasma cells, as the cytoplasm of both plasma cell types was strongly increased by an extended network of the ER (Fig. 5 E and Fig. S4 D). While the stacking of the ER appeared slightly less tight in Pax5-expressing plasma cells, the cytosolic surfaces of the ER were similarly densely occupied with ribosomes, as shown at higher magnification (Fig. 5 E and Fig. S4 D). To measure the increase of the ER network by a second independent method, we stained plasma cells from the bone marrow of 6–8-mo-old mice with the

ER-Tracker Red dye. Surprisingly, flow-cytometric analysis revealed that the intensity of the ER-Tracker staining was moderately increased in $Igh^{Pax5/+}$ plasma cells compared with control $Igh^{+/+}$ plasma cells (Fig. S4 E). In summary, we conclude that Pax5 expression did not interfere with the formation of a functional secretory apparatus in plasma cells.

Impaired CSR to IgG1 in $Igh^{Pax5/+}$ mice

We next investigated the potential of $Igh^{Pax5/+}$ B cells to undergo CSR to IgG under in vitro and in vivo conditions. For this, we stimulated naive splenic B cells for 4 d with LPS or anti-CD40, IL-4, and IL-5 to induce CSR to IgG3 or IgG1, respectively (Fig. 6, A and B). Under both conditions, $Igh^{Pax5/+}$ B cells underwent CSR to IgG3 and IgG1 at similar frequency as control $Igh^{+/+}$ B cells (Fig. 6, A and B), indicating that ectopic Pax5 expression in B cells did not interfere with CSR under in vitro stimulation conditions. However, the analysis of GC B cells ($CD19^+GL7^+Fas^+$) at day 14 after immunization with NP-KLH (in alum) revealed a 1.8-fold decrease of GC B cells in the spleen of $Igh^{Pax5/+}$ mice compared with control $Igh^{+/+}$ littermates (Fig. 6 C). While the antigen-specific (NP^+) cell fraction within the GC B cell population was similar, the fraction of IgG1-switched cells within the NP^+ GC B cell population was 2.9-fold reduced in $Igh^{Pax5/+}$ mice compared with control littermates (Fig. 6 C). A similar result was obtained upon immunization with sheep RBCs (SRBCs), which elicits a strong polyclonal B cell response (Fig. S5 A). At day 14 after immunization with this antigen, GC B cells were present at a similar frequency in the spleen of $Igh^{Pax5/+}$ and $Igh^{+/+}$ mice, while the frequency of $IgG1^+$ GC B cells was still twofold reduced in $Igh^{Pax5/+}$ mice compared with control littermates (Fig. S5 A). Together, these data indicate that ectopic Pax5 expression interfered with CSR to IgG1 in vivo, but not under in vitro conditions.

We hypothesize that the in vivo versus in vitro discrepancy is likely explained by the complex GC microenvironment consisting of several cell types that support the activation and differentiation of B cells upon cognate antigen interaction. In particular, CSR and GC B cell differentiation require the interaction with T follicular helper (T_{FH}) cells (Crotty, 2019). Upon recruitment to the GC, the T_{FH} cells provide signals to B cells through their costimulatory surface molecules CD40L and ICOS (CD278) as well as through secretion of the cytokines IL-4 and IL-21 (Crotty, 2019). At 14 d after NP-KLH immunization, T_{FH} cells were present at normal numbers in splenic GCs of $Igh^{Pax5/+}$ mice (Fig. 6 D). As observed for all T cells, the T_{FH} cells of $Igh^{Pax5/+}$ mice also exhibited ectopic and variegated expression of Pax5 (Fig. 6 D). It is therefore conceivable that ectopic Pax5 expression may impair the function of the T_{FH} cells, thus leading to impaired CSR in $Igh^{Pax5/+}$ mice.

The presence of normal T cells rescues CSR in $Igh^{Pax5/+}$ B cells

As the T_{FH} cells ectopically expressed Pax5 in $Igh^{Pax5/+}$ mice, we next examined whether the CSR defect of these mice was B cell–intrinsic or dependent on the Pax5-expressing T_{FH} cells. To this end, we generated mixed bone marrow chimeras by reconstituting lethally irradiated C57BL/6 mice with a 1:1 mixture of $Igh^{Pax5/+}$ and $Igh^{\Delta Jh/\Delta Jh}$ (J_HT) bone marrow (Fig. S5 B). All B cells in these chimeric mice originated from the $Igh^{Pax5/+}$ stem cells, as the homozygous J_HT mutation, eliminating the D_HQ52, J_H and Eμ elements of the *Igh* locus (Gu et al., 1993), prevented B cell development of the J_HT progenitors. In contrast, all T cells should be derived from the J_HT stem cells, as the $Igh^{Pax5/+}$ progenitors cannot contribute to T lymphopoiesis in a competitive setting due to a partial block of thymic T cell development in $Igh^{Pax5/+}$ mice (Souabni et al., 2007). For comparison, we generated bone marrow chimeras with a mixture of $Igh^{+/+}$ and J_HT bone marrow and, 3 mo after transplantation, immunized all chimeric mice with SRBCs, followed by flow-cytometric analysis after 14 d (Fig. S5 B). The T_{FH} cells in the experimental $Igh^{Pax5/+}$ chimeric mice did not express Pax5 and were thus of J_HT origin (Fig. S5 C). Notably, the $IgG1^+$ GC B cells were present at similar frequencies in the spleen of experimental $Igh^{Pax5/+}$ and control $Igh^{+/+}$ chimeric mice (Fig. S5 D), indicating that the decrease of $IgG1^+$ GC B cells in $Igh^{Pax5/+}$ mice (Fig. S5 A) was not a B cell–intrinsic defect.

In addition, we performed an adoptive cell transfer experiment by coinjecting splenic $Igh^{B1\text{-}8hi/Pax5}$ $Prdm1^{Gfp/+}$ B cells ($CD45.1^+CD45.2^+$) and OT-II TCR-transgenic $Rag2^{-/-}$ $CD4^+$ T cells ($CD45.2^+$) into C57BL/6 mice ($CD45.1^+$; Fig. 7 A). The $Igh^{B1\text{-}8hi}$ allele expresses the NP-specific high-affinity BCR B1-8^{hi} (Shih et al., 2002), and the OT-II transgene expresses an OVA-specific TCR (Barnden et al., 1998). In the context of this experiment, it is important to note that Pax5 was not expressed in T_{FH} cells derived from OT-II TCR-transgenic $Rag2^{-/-}$ $CD4^+$ T cells. Control cell transfer experiments were performed with $Igh^{B1\text{-}8hi/+}$ $Prdm1^{Gfp/+}$ B cells ($CD45.1^+CD45.2^+$; Fig. 7 A). 1 d after injection, the mice were immunized with the NP-OVA antigen (in alum) and analyzed by flow cytometry and ELISPOT assay 6 d after immunization. Analyses of the transferred $CD45.1^+CD45.2^+$ B cells and their GFP^+ plasma cell progeny revealed similar frequencies of total and $IgG1^+$ GC B cells (Fig. 7 B) as well as GFP^+ plasma cells (Fig. 7 C) in the spleen of mice injected with experimental ($Igh^{B1\text{-}8hi/Pax5}$) or control ($Igh^{B1\text{-}8hi/+}$) B cells. The numbers of NP-IgM and NP-IgG1 ASCs was minimally reduced in the experimental compared with the control setting (Fig. 7 D). The ELISPOT size of experimental NP-IgM and NP-IgG1 ASCs was 1.5- and 1.9-fold reduced compared with control ASCs, respectively, thus further indicating a minor defect of antibody secretion in Pax5-expressing plasma cells. In summary, these experiments indicate that CSR to IgG was rescued in $Igh^{Pax5/+}$ B cells in the presence of functional T cells, which resulted in normalized numbers of IgG-secreting plasma cells.

Normal B cell immune responses in Peyer's patches of $Igh^{Pax5/+}$ mice

Since we observed that the B cell immune responses in $Igh^{Pax5/+}$ mice are restored in the presence of functional T cells, we predicted that immunization with the T cell–independent TNP-Ficoll antigen should give rise to normal CSR and plasma cell development in $Igh^{Pax5/+}$ mice. Indeed, total and $IgG2b^+$ plasma cells ($TACI^+CD138^+$) were present at similar frequencies in the spleen of $Igh^{Pax5/+}$ and $Igh^{+/+}$ mice at day 14 after TNP-Ficoll immunization (Fig. 8 A). Consistent with this result, the level of *Ighg2b* transcripts was also similar in bone marrow plasma cells of both genotypes (Fig. S4 C). We next analyzed Peyer's patches,

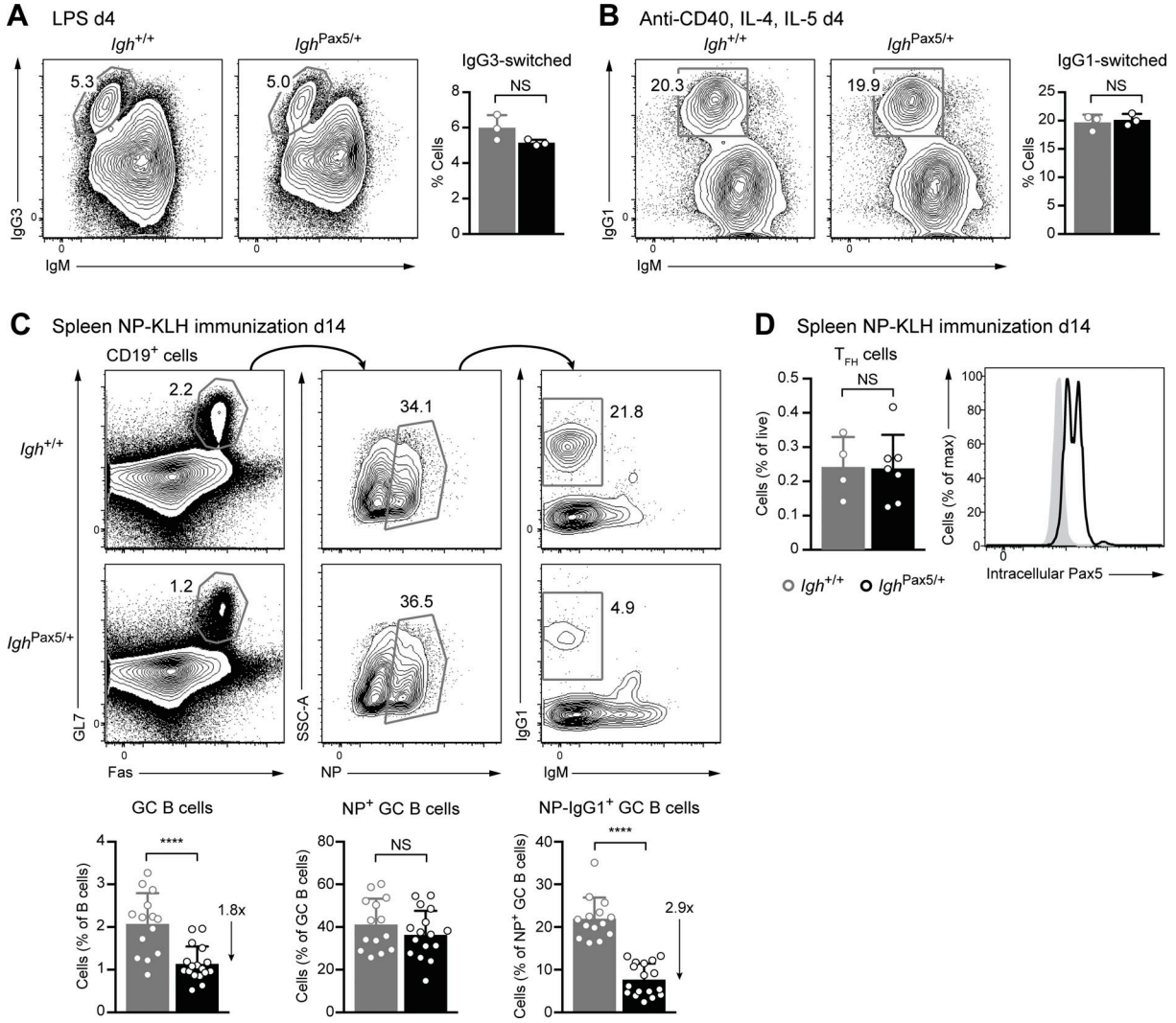

Figure 6. **Impaired CSR to IgG1 in *Igh*$^{Pax5/+}$ mice. (A and B)** Normal CSR to IgG3 and IgG1 under in vitro conditions. Naive B cells from the spleen and lymph nodes of *Igh*$^{Pax5/+}$ (black) or *Igh*$^{+/+}$ (gray) mice were cultured for 4 d with LPS (A) or anti-CD40, IL-4, and IL-5 (B) before flow-cytometric analysis and quantification of the class-switched B cells. The data are representative of two (A) or three (B) independent experiments. **(C)** GC B cell response in the spleen of *Igh*$^{Pax5/+}$ and *Igh*$^{+/+}$ mice 14 d after immunization with NP-KLH (in alum). The frequencies of total GC B cells (CD19$^+$GL7$^+$Fas$^+$), NP-specific GC B cells, and NP-specific IgG1$^+$ GC cells were determined by flow cytometry (above) and quantified (below). The data are pooled from four independent experiments. **(D)** Frequency of T_{FH} cells (CD4$^+$CXCR5$^+$PD1$^+$Bcl6$^+$) in the spleens of *Igh*$^{Pax5/+}$ (black) and *Igh*$^{+/+}$ (gray) mice 14 d after NP-KLH immunization (left). Flow-cytometric analysis of Pax5 expression in T_{FH} cells from the *Igh*$^{Pax5/+}$ (black line) and *Igh*$^{+/+}$ (gray filled) spleen is shown on the right. The data are pooled from two independent experiments. Statistical data (A–D) are shown as mean values with SD and were analyzed by the two-tailed unpaired Student's *t* test; ****, P < 0.000. NS, not significant (P > 0.05). Each dot corresponds to one mouse. SSC-A, side scatter area.

as CSR to IgA in these gut-associated lymphoid organs is also known to be T cell–independent (Bergqvist et al., 2010). Total and IgA-switched GC B cells were present in similar number in the Peyer's patches of *Igh*$^{Pax5/+}$ and *Igh*$^{+/+}$ mice (Fig. 8 B). Moreover, total and IgA$^+$ plasma cells were equally abundant in Peyer's patches of both genotypes (Fig. 8 C). Hence, these data provide further evidence that ectopic Pax5 expression in the B cell lineage does not interfere with CSR, GC B cell formation, and plasma cell development.

Discussion

The distinct gene expression programs of B cells and plasma cells are controlled by different transcription factors as exemplified by the mutually exclusive expression of Pax5 and Blimp1 and their cross-antagonism in B cell and plasma cell development, respectively (Nutt et al., 2015). In addition, ectopic expression of Pax5 in in vitro cultured B cells was shown to prevent plasmablast differentiation (Lin et al., 2002; Usui et al., 1997). Together, these observations led to the commonly held view that plasma cell differentiation strictly depends on the repression of *Pax5* (Nutt et al., 2015). Here, we challenged this hypothesis by investigating the development of plasma cells in the *Igh*$^{Pax5/+}$ mouse model, which demonstrated, contrary to expectation, that ectopic Pax5 expression from the *Igh* locus is compatible with efficient development of plasmablasts and plasma cells, as discussed below.

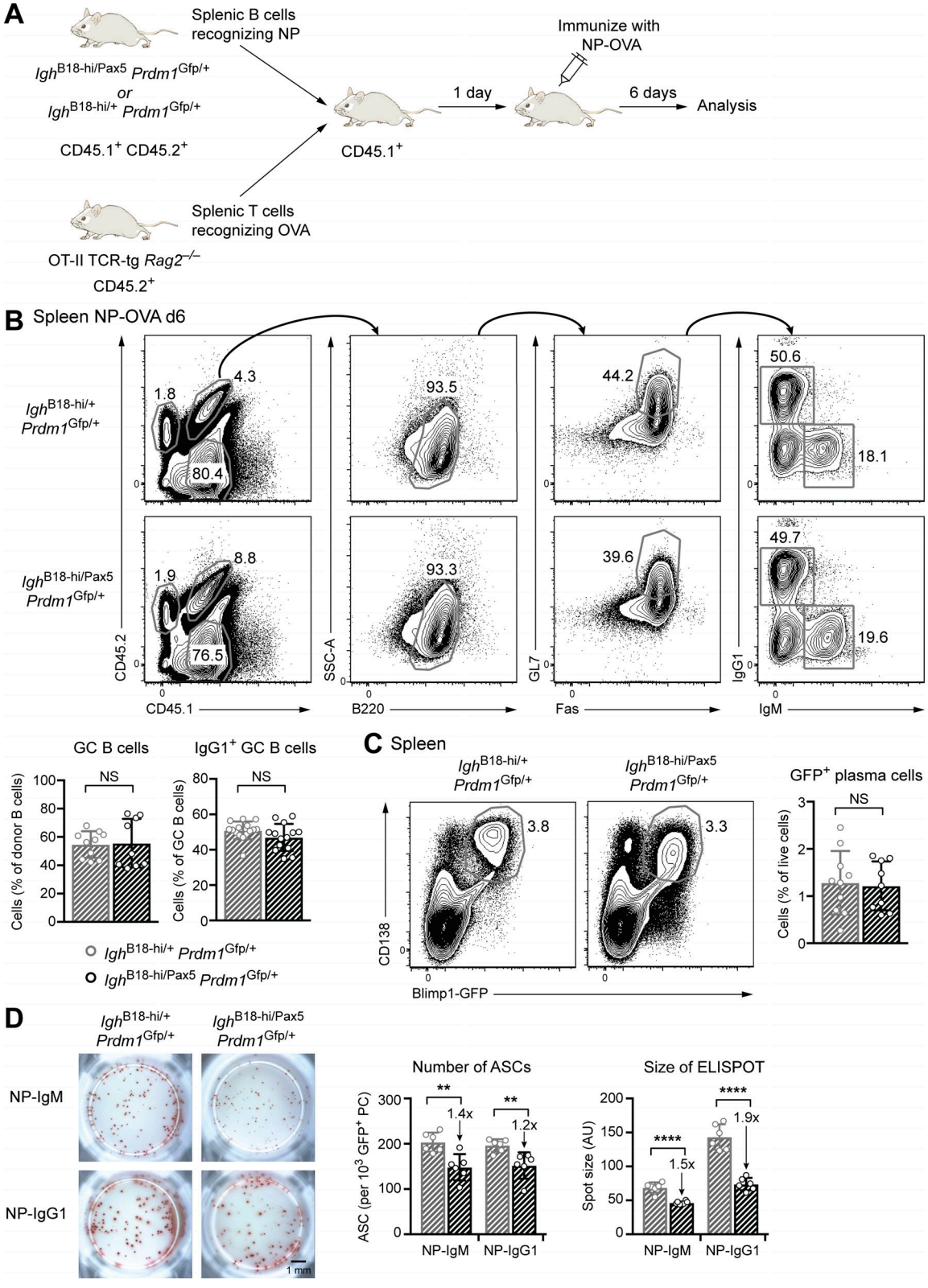

Figure 7. **Rescue of IgG1 CSR in the presence of functional T cells. (A)** Experimental strategy to interrogate B-lineage–intrinsic effects of ectopic Pax5 expression in response to immunization. CD43⁻ B cells isolated from the spleens of *Igh*$^{B1\text{-}8hi/Pax5}$ *Prdm1*$^{Gfp/+}$ or *Igh*$^{B1\text{-}8hi/+}$ *Prdm1*$^{Gfp/+}$ mice (CD45.1⁺CD45.2⁺) were cotransferred with splenic T cells from OT-II TCR-tg *Rag2*$^{-/-}$ mice (CD45.2⁺) into C57BL/6 recipients (CD45.1⁺). 1 d after cell transfer, the recipients were immunized with NP-OVA (in alum) and were analyzed 6 d after immunization. **(B)** Flow-cytometric analysis of splenic GC B cells of *Igh*$^{B1\text{-}8hi}$ donor origin. The frequencies of IgG1⁺ GC B cells of the *Igh*$^{B1\text{-}8hi/+}$ *Prdm1*$^{Gfp/+}$ and *Igh*$^{B1\text{-}8hi/Pax5}$ *Prdm1*$^{Gfp/+}$ genotypes were determined by sequential gating on donor cells (CD45.1⁺CD45.2⁺), B cells (B220⁺), and GC B cells (GL7⁺Fas⁺) by flow cytometry (above). The quantification of the frequencies of GC B cells and IgG1⁺ GC B cells

is shown below. The data are pooled from three independent experiments. **(C)** Analysis of splenic GFP$^+$ plasma cells derived from the transferred *Igh*$^{B1\text{-}8hi/+}$ *Prdm1*$^{Gfp/+}$ or *Igh*$^{B1\text{-}8hi/Pax5}$ *Prdm1*$^{Gfp/+}$ B cells. The flow-cytometric analysis is shown on the left, and the frequency of the GFP$^+$ plasma cells is quantified on the right. The data are pooled from two independent experiments. **(D)** ELISPOT assay to determine the frequency of anti–NP-IgM and anti–NP-IgG1 ASCs derived from the transferred *Igh*$^{B1\text{-}8hi/+}$ *Prdm1*$^{Gfp/+}$ or *Igh*$^{B1\text{-}8hi/Pax5}$ *Prdm1*$^{Gfp/+}$ cells. Six days after immunization with NP-OVA, 500 GFP$^+$CD138$^+$ plasma cells of donor origin were directly sorted onto NP_{20}-BSA–coated plates. Cells were incubated for 6 h, before the number and size of anti–NP-IgM and anti–NP-IgG1 ELISPOTs were determined. Images of representative ELISPOT wells (left), the mean cell number (middle), and the median ELISPOT size (right) are shown for anti–NP-IgM and anti–NP-IgG1 ASCs. Statistical data (B–D) are shown as mean values with SD and were analyzed by the two-tailed unpaired Student's *t* test; **, P < 0.01; ****, P < 0.0001. NS, not significant (P > 0.05). Each dot (B–D) corresponds to one mouse. A scale bar of 1 mm length is shown.

While Pax5 is similarly expressed during B cell development in *Igh*$^{Pax5/+}$ mice as in control littermates, its expression and genome-wide binding are maintained at a high level only in plasmablasts and plasma cells of the *Igh*$^{Pax5/+}$ mice. As a consequence, the ectopically expressed Pax5 protein activates or represses many genes that are normally down- or up-regulated in plasma cells, respectively. Notably, one third of the deregulated and Pax5-bound genes in *Igh*$^{Pax5/+}$ plasma cells were previously identified as activated or repressed Pax5 target genes in pro-B or mature B cells (Delogu et al., 2006; Revilla-I-Domingo et al., 2012; Schebesta et al., 2007; Table S2). Despite the large gene expression changes, the key plasma cell regulators Blimp1, Irf4,

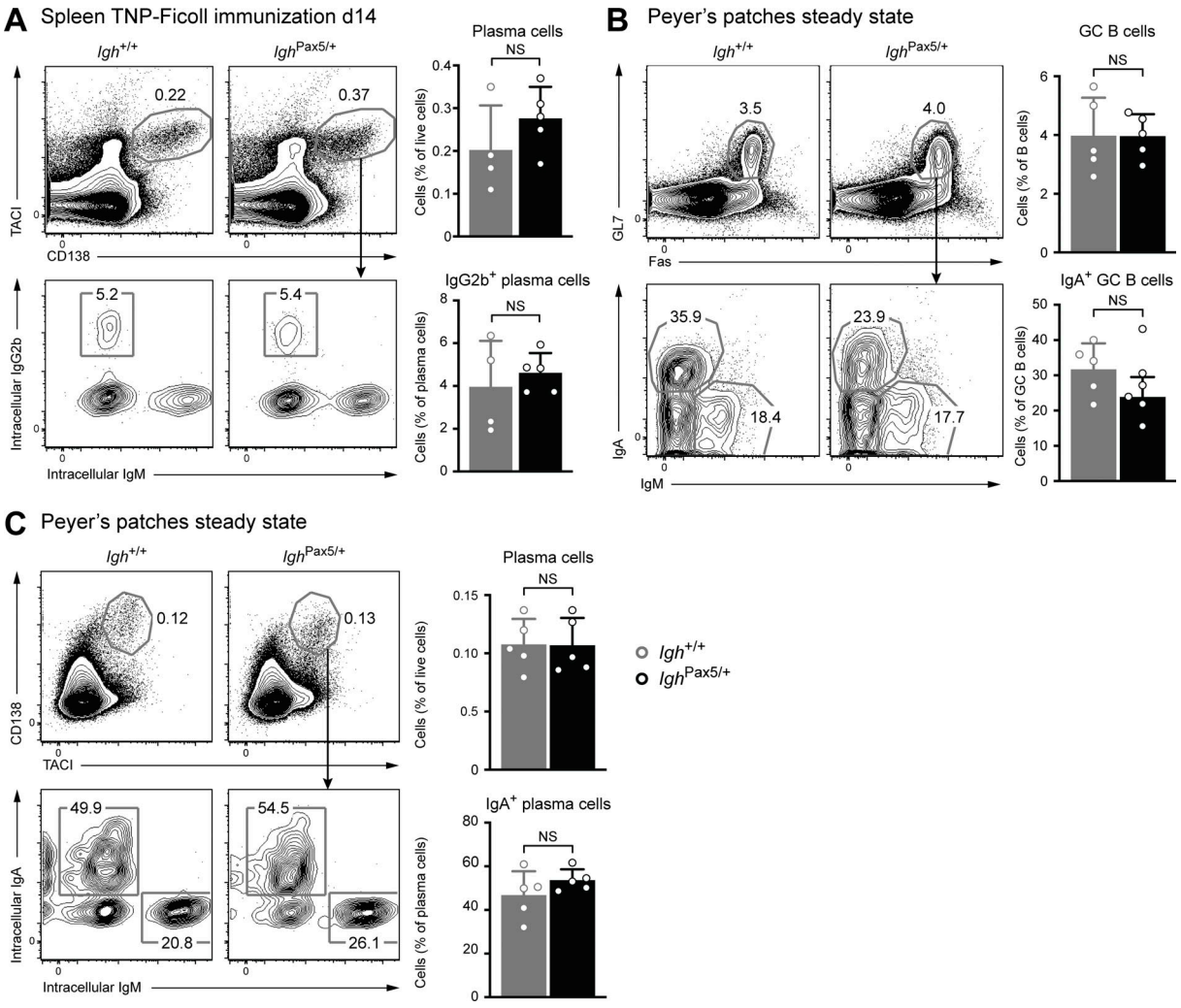

Figure 8. **Normal CSR and plasma cell development under T cell–independent stimulation conditions. (A)** Flow-cytometric analysis of plasma cells (TACI$^+$CD138$^+$; upper row) in the spleen of *Igh*$^{Pax5/+}$ and *Igh*$^{+/+}$ littermates 14 d after immunization with TNP-Ficoll. The frequency of IgG2b-expressing plasma cells was determined by intracellular IgG2b staining (lower row). The results shown are representative of two experiments. **(B)** Normal generation of GC B cells in the Peyer's patches of *Igh*$^{Pax5/+}$ and *Igh*$^{+/+}$ littermates at steady state. The frequencies of total GC B cells (CD19$^+$GL7$^+$Fas$^+$) and IgA$^+$ GC cells were determined by flow cytometry (left) and quantified (right). **(C)** Normal generation of IgA-expressing plasma cells in the Peyer's patches at steady state. The frequencies of total (TACI$^+$CD138$^+$) and IgA-expressing plasma cells were determined by flow cytometry (left) and quantified (right). One experiment (B and C) was performed. Statistical data (A–C) are shown as mean values with SD and were analyzed by the two-tailed unpaired Student's *t* test; NS, not significant (P > 0.05). Each dot corresponds to one mouse. TACI, transmembrane activator CAML interactor.

E2A, E2-2, and Ikaros are similarly expressed in $Igh^{Pax5/+}$ and control plasma cells. Consistent with this finding, the $Igh^{Pax5/+}$ mice undergo efficient plasma cell development under steady-state conditions and in response to immunization. These data indicate first and foremost that plasma cell development can occur in the absence of *Pax5* repression, contrary to the currently held dogma. Second, Pax5-expressing plasma cells exhibit normal trafficking and homing from secondary lymphoid organs to their survival niches in the bone marrow. The discrepancy between earlier published data and our current results may be explained by the fact that the effect of ectopic Pax5 expression was previously analyzed by transfection in in vitro cultured B cells in contrast to our in vivo analysis of the more physiological $Igh^{Pax5/+}$ mouse model.

The initiation of plasmablast differentiation in the presence of continuous Pax5 expression was an unexpected result, as Pax5 is known to transcriptionally repress the expression of the essential plasma cell regulator Blimp1 in mature B cells (Delogu et al., 2006; Revilla-I-Domingo et al., 2012). In addition to Pax5, other transcription factors such as Bach2, SpiB (*Spib*), Irf8, and c-Rel (*Rel*) also contribute to the repression of the *Prdm1* gene in B cells (Carotta et al., 2014; Ochiai et al., 2006; Roy et al., 2019; Willis et al., 2017). Although Pax5 activated the expression of these repressors also in $Igh^{Pax5/+}$ plasma cells, Blimp1 expression remained normal in these cells. On the other hand, multiple transcription factors including Irf4, Stat3, RelA (Rela), E2A (Tcf3), and E2-2 (Tcf4) are required to activate the *Prdm1* gene at the onset on plasmablast differentiation (Klein et al., 2006; Kwon et al., 2009; Roy et al., 2019; Sciammas et al., 2006; Wöhner et al., 2016). Notably, B cells that undergo strong BCR and CD40 signaling in the light zone of the GC first activate the *Irf4* gene to become plasmablast precursors before the initiation of *Prdm1* expression in plasmablasts (Ise et al., 2018). It is therefore conceivable that the increased expression of the activator Irf4 can override the Pax5-mediated repression of *Prdm1* during the B cell–to–plasmablast transition. Once expressed, Irf4 and Blimp1 subsequently control the plasma cell fate regardless of ectopic Pax5 expression, indicating that these plasma cell regulators are dominant over Pax5 in plasma cells.

One complication of the $Igh^{Pax5/+}$ mouse model is the fact that ectopic and variegated expression of Pax5 is also observed in the T cell lineage of this mouse strain, including the T_{FH} cells (Souabni et al., 2007; this study). It is therefore not surprising that the $Igh^{Pax5/+}$ mice exhibit impaired CSR to IgG and GC B cell differentiation, as both pathways strictly depend on functional T_{FH} cells (Crotty, 2019). Replacing the dysfunctional $Igh^{Pax5/+}$ T_{FH} cells with wild-type $Igh^{+/+}$ T_{FH} cells in competitive cell transfer experiments resulted in normal numbers of $IgG1^+$ $Igh^{Pax5/+}$ GC B cells in response to immunization, indicating that the observed CSR and GC B cell defects are indeed not B cell–autonomous. In contrast, the moderate defect of IgG1 secretion by $Igh^{Pax5/+}$ plasma cells is B cell–intrinsic, while the secretion of IgM is normal, consistent with the finding that Pax5-expressing plasma cells exhibit a morphology characterized by an extended ER network similar to wild-type plasma cells. The Fc regions of the different IgG isotypes are known to specifically undergo fucosylation, which is catalyzed by the fucosyltransferase Fut8 in the ER (Li et al., 2015). Fut8 is known to be required for efficient secretion of the different IgG isotypes (Li et al., 2015). In this context, it is interesting to note that Pax5 directly represses the *Fut8* gene fourfold in $Igh^{Pax5/+}$ plasma cells (Fig. S3 F). These data therefore suggest that the Pax5-dependent repression of *Fut8* may be responsible for the impaired IgG secretion of $Igh^{Pax5/+}$ plasma cells.

While young $Igh^{Pax5/+}$ mice have modestly elevated levels of long-lived plasma cells in the bone marrow compared with control mice, the Pax5-expressing plasma cells are skewed toward the less mature Blimp1-GFP^{int} phenotype (Kallies et al., 2004). Moreover, the number of total as well as mature Blimp1-GFP^{hi} plasma cells decreases with progressing age in $Igh^{Pax5/+}$ mice, demonstrating that ectopic Pax5 expression interferes with the longevity of plasma cells in the bone marrow. Notably, the Bcl-2 family member Mcl-1, which is essential for the survival of plasma cells in the bone marrow (Peperzak et al., 2013), is normally expressed in Pax5-expressing plasma cells. As the cell surface lectin CD93 is also required for the persistence of plasma cells in the bone marrow niche (Chevrier et al., 2009), it is conceivable that the fivefold repression of *Cd93* expression by Pax5 (Fig. 2 E and Fig. S3 E) may contribute to the impaired longevity of $Igh^{Pax5/+}$ plasma cells.

In summary, our study has unequivocally demonstrated that antibody-secreting plasma cells can robustly develop even in the absence of *Pax5* repression. However, *Pax5* repression is required to ensure efficient IgG secretion and normal accumulation of long-lived plasma cells with progressing age.

Materials and methods

Mice

The following mice were maintained on the C57BL/6 genetic background: $Igh^{P5ki/+}$ (Souabni et al., 2007), $Igh^{Pax5/+}$ (this study), $Prdm1^{Gfp/+}$ (Kallies et al., 2004), J_HT (Gu et al., 1993), $Igh^{B1\text{-}8hi/B1\text{-}8hi}$ (Shih et al., 2002), $Rag2^{-/-}$ (Shinkai et al., 1992), OT-II TCR-tg (Barnden et al., 1998), and transgenic Flpe mice (Rodríguez et al., 2000). All animal experiments were performed according to valid project licenses, which were approved and regularly controlled by the Austrian Veterinary Authorities.

Antibodies

The following monoclonal antibodies were used for flow cytometry: B220/CD45R (RA3-6B2), CD2 (RM2-5), CD4 (GK1.5), CD8α (53–6.7), CD19 (1D3), CD21 (7G6), CD22 (Cy34.1), CD23 (B3B4), CD45.1 (A20), CD45.2 (104), CD49b/Itga2 (DX5), CD93 (AA4.1), CD95/Fas (Jo2), CD117/Kit (2B8), CD138 (281–2), GL7 (GL7), CD267/TACI (8F10), IgA (mA-6E1), IgD (11-26c.2a), IgM (II/41), IgG1 (A85-1), IgG2b (R12-3), IgG3 (R40-82), Sca1/Ly6a (D7), TCRβ (H57-597), CD185/Cxcr5 (REA215), and PD1 (REA802). The following monoclonal antibodies were used for intracellular flow cytometry: Pax5 (1H9) and Bcl6 (K112-91). NP-BSA-biotin was obtained from Biosearch Technologies. The ER content of B lymphocytes was determined by staining with the ER-Tracker Red dye (BODIPY TR Glibenclamide; Invitrogen).

The following antibody was used for ChIP-seq analysis: anti-Pax5 (rabbit polyclonal antibody, detecting the paired domain;

amino acids 17–145; Adams et al., 1992; Busslinger laboratory). The following antibodies were used for ELISPOT and ELISA: goat anti-mouse IgM, IgG, IgG1, IgG2b, and IgA (human adsorbed; SouthernBiotech), HRP-coupled goat anti-mouse IgM, IgG, and IgG1 (human adsorbed; SouthernBiotech), and AP-coupled goat anti-mouse IgM, IgG1, IgA, and IgE (human adsorbed; SouthernBiotech).

Definition of cell types by flow cytometry

Pro-B cells ($B220^+CD19^+Kit^+CD2^-IgM^-$), pre-B cells ($B220^+CD19^+Kit^-CD2^+IgM^-$), immature B cells ($B220^+CD19^+IgM^+IgD^-$), recirculating B cells ($B220^+CD19^+ IgM^{lo}IgD^{hi}$), follicular B cells ($B220^+CD19^+CD23^{hi}CD21^{lo}$), marginal zone B cells ($B220^+CD19^+CD21^{hi}CD23^{lo}$), GC B cells ($CD19^+B220^+GL7^+Fas^+$), in vitro activated B cells ($B220^+CD22^+CD138^-$Blimp1-GFP^-), in vitro cultured plasmablasts ($CD22^-CD138^+$Blimp1-GFP^+), plasma cells ($Lin^-[CD4^-CD8^-CD21^-CD49b^-]B220^{int}CD138^+$Blimp1-$GFP^+$), T_{FH} cells ($CD4^+CXCR5^+PD1^+Bcl6^+$). Flow cytometry experiments and FACS sorting were performed on LSR Fortessa (BD Biosciences) and FACSAria III (BD Biosciences) machines, respectively. FlowJo software (Treestar) was used for data analysis.

Generation of bone marrow chimeras

Bone marrow cells from J_HT, $Igh^{Pax5/+}$ $Prdm1^{Gfp/+}$, and $Igh^{+/+}$ $Prdm1^{Gfp/+}$ mice were enriched for hematopoietic progenitors by immunomagnetic depletion of cells expressing the cell surface markers CD4, CD8, CD21, and CD49b. Progenitor cells from $Igh^{Pax5/+}$ $Prdm1^{Gfp/+}$ and $Igh^{+/+}$ $Prdm1^{Gfp/+}$ mice were mixed in a 1:1 ratio with progenitor cells from J_HT mice before intravenous injection into lethally irradiated (2 × 5.5 Gy) J_HT recipients. The mice were immunized 3 mo after bone marrow reconstitution.

Adoptive transfer of B and T cells

$CD43^-$ B cells from the spleen of $Igh^{B1\text{-}8hi/Pax5}$ $Prdm1^{Gfp/+}$ and $Igh^{B1\text{-}8hi/+}$ $Prdm1^{Gfp/+}$ mice ($CD45.1^+$ $CD45.2^+$) were isolated by immunomagnetic depletion with CD43-MicroBeads (Miltenyi Biotec). $CD4^+$ T cells from the spleen of OT-II TCR-tg $Rag2^{-/-}$mice ($CD45.2^+$) were selected by immunomagnetic depletion of $CD11b^+$, $CD11c^+$, and $CD115^+$ myeloid cells. Approximately 3 × 10^6 B cells and 5 × 10^5 T cells from the respective donors were transferred intravenously into C57BL/6 recipients ($CD45.1^+$).

Intracellular Pax5 staining

Pax5 staining was performed with a monoclonal anti-Pax5 antibody (1H9; BioLegend) after fixation and permeabilization with the Foxp3/transcription factor staining buffer set (eBioscience).

In vitro B cell stimulation experiments

Mature B cells from spleen and lymph nodes were isolated as $CD43^-$ B cells by immunomagnetic sorting with CD43-MicroBeads (Miltenyi Biotec). For LPS stimulation, mature B cells were seeded at a density of 5 × 10^5 cells/ml in IMDM medium containing 10% FCS (A15-101; GE Healthcare), 1 mM glutamine, 50 µM β-mercaptoethanol, and 25 µg/ml LPS (L4130; Sigma-Aldrich) for 4 d. For anti-CD40 plus IL-4 and IL-5 stimulation experiments, mature B cells were plated at 5 × 10^5 cells/ml in IMDM medium supplemented with 10% FCS, 1 mM glutamine, and 50 µM β-mercaptoethanol, and containing anti-CD40 antibody (2 µg/ml; HM40-3; eBioscience), IL-4 (20 ng/ml), and IL-5 (10 ng/ml) for 4 d.

Immunization

The immune response to a T cell–dependent antigen was studied by intraperitoneal injection of 100 µg NP-KLH (Biosearch Technologies) in alum, or 100 µg of NP conjugated to OVA (NP-OVA; Biosearch Technologies) in alum. To investigate the response to a polyclonal antigen, SRBCs were washed in PBS and resuspended at 10^9 cells/ml followed by intraperitoneal injection of 100 µl into an adult mouse. GC B cells and plasma cells were analyzed by flow cytometry 6–14 d after immunization. The immune response to a T cell–independent antigen was studied by intraperitoneal injection of 10 µg of TNP-Ficoll (Biosearch Technologies) in PBS and by flow-cytometric analysis 14 d after immunization.

ELISPOT analysis

The frequencies of ASCs were determined by ELISPOT assay as described (Smith et al., 1997). ELISPOT plates (Merck) coated with goat anti-mouse IgM or IgG antibody (SouthernBiotech) were used for capturing total IgM or IgG antibodies, respectively, which were secreted by ASCs in the bone marrow of nonimmunized mice at steady state. Alternatively, NP-BSA–coated ELISPOT plates were used for capturing NP-specific antibodies secreted by splenic ASCs from immunized mice. Cells from bone marrow or spleen were treated with the ACK lysing buffer (Thermo Fisher Scientific) before incubation for 6 h at 37°C in ELISPOT wells at 2 × 10^5 cells/well (steady state) or 2 × 10^6 cells/well (after immunization). 6 d after NP-OVA immunization (Fig. 7 D), $CD138^+GFP^+$ plasma cells were directly sorted into ELISPOT wells at 500 cells/well before incubation. ELISPOTs were visualized with goat anti-mouse IgM, IgG, or IgG1 antibodies conjugated to HRP (SouthernBiotech), and color was developed by addition of the AEC staining reagents (Sigma-Aldrich). After extensive washing, the spots were counted with an ELISPOT Reader System (Autoimmun Diagnostika).

Measurement of ELISPOT size

The size of all ELISPOTs in each well was analyzed using a macro developed in Fiji macro language to perform automated segmentation and measurement in batch mode. Borders of the well area were defined to exclude outside reflections from the analysis, and then color deconvolution was used to separate ELISPOTs from background. Laplace filtering and background subtraction were used to enhance contrast and create binary images of the objects. Segmentation was performed in three rounds to cover different sizes, and the resulting images were then merged. The segmented images were then refined, and objects with low contrast were excluded. The resulting areas were measured.

ELISA measurements

Serum titers of total IgM, IgG1, IgA, and IgE in unimmunized mice were determined by ELISA (Smith et al., 1997). ELISA plates (Sigma-Aldrich) were coated with goat anti-mouse IgM,

IgG1, IgA, and IgE antibody (human adsorbed; SouthernBiotech) before sera was incubated at 4°C for 16 h. Sera antibody concentrations were determined by addition of goat anti-mouse IgM, IgG1, IgA, and IgE antibodies conjugated to alkaline phosphatase (human adsorbed, SouthernBiotech), and color was developed by addition of pNPP One Component Microwell Substrate Solution (SouthernBiotech). The color intensity was quantified using an Epoch Microplate Spectrophotometer (BioTek), using a standard consisting of a mixture of all the sera analyzed.

Electron microscopy

Plasma cells from the bone marrow were isolated by enrichment of CD138$^+$ cells using immunomagnetic beads (STEMCELL Technologies), followed by flow cytometry sorting of CD138$^+$ GFP$^+$ plasma cells. Plasma cells were fixed using 2.5% glutaraldehyde in 0.1 M sodium phosphate buffer, pH 7.4, for 1 h at room temperature. Due to the low numbers of plasma cells, the pelleted cells were mixed with 3% agarose and cut into small pieces. Samples were post-fixed in 2% osmium tetroxide in 0.1 M sodium phosphate buffer on ice and dehydrated in a graded series of acetone on ice before embedding in Agar 100 resin. Subsequently, 70-nm sections were cut parallel to the substrate and post-stained with 2% uranyl acetate and Reynolds lead citrate. Sections were examined with a FEI Morgagni 268D (FEI) operated at 80 kV. Images were acquired using an 11-megapixel Morada charge-coupled device camera (Olympus-SIS).

ChIP analysis of Pax5

In vitro activated B cells and plasmablasts derived by LPS stimulation from *Igh*$^{Pax5/+}$ and *Igh*$^{+/+}$ B cells, and DT40 chicken cells were separately cross-linked with 1% formaldehyde (Sigma-Aldrich) for 10 min. Nuclei were prepared and lysed in the presence of 0.25% SDS, and chromatin was sheared by sonication with the Bioruptor Standard (Diagenode). Murine chromatin samples were mixed with 10% of chicken DT40 chromatin, followed by immunoprecipitation with a polyclonal antibody recognizing the conserved paired domain of Pax5 (Adams et al., 1992). Specific enrichment was measured and calculated as the precipitated DNA amount relative to input DNA. The ChIP-precipitated DNA (0.5–1 ng) was used for library preparation and subsequent Illumina deep sequencing.

cDNA preparation for RNA-seq

Plasma cells (CD138$^+$GFP$^+$) were sorted from the bone marrow as described in Fig. S3 A, and plasmablasts were isolated by flow-cytometric sorting as CD22$^-$CD138$^+$GFP$^+$ cells after 4 d of LPS stimulation of B cells from the spleen and lymph nodes. Total RNA from in vitro stimulated plasmablasts or ex vivo sorted plasma cells was isolated with the RNeasy Plus Mini Kit (Qiagen), and mRNA was purified by two rounds of poly(A) selection with the Dynabeads mRNA purification kit (Invitrogen). The mRNA was fragmented by heating at 94°C for 3 min in fragmentation buffer. The fragmented mRNA was used as template for first-strand cDNA synthesis with random hexamers and the Superscript Vilo First-Strand Synthesis System (Invitrogen). The second-strand cDNA synthesis was performed with 100 mM deoxy ATP (dATP), dCTP, dGTP, and dUTP in the presence of RNase H, *Escherichia coli* DNA polymerase I, and DNA ligase (Invitrogen). The incorporation of dUTP allowed for specific elimination of the second DNA strand during library preparation, thereby preserving strand specificity (Parkhomchuk et al., 2009).

Library preparation and Illumina deep sequencing

0.5 ng to 1 µg of cDNA or ChIP-precipitated DNA was used as starting material for the generation of sequencing libraries with the NEBNext Ultra II DNA library prep kit for Illumina (NEB). Cluster generation and sequencing were performed using the Illumina HiSeq 2500 system with a read length of 50 nucleotides, according to the manufacturer's guidelines.

Database of RefSeq-annotated genes

The database generation of RefSeq-annotated genes was performed as previously described (Wöhner et al., 2016). To refine the annotation of immunoglobulin genes, the immunoglobulin λ light-chain segments were replaced with their corresponding converted GRCm38.p3 annotations (Ensembl version 79; Yates et al., 2016). The resulting number of genes was 24,732.

Processing of Pax5 ChIP-seq data

All reads that passed a basic quality control filter (Illumina chastity) were further processed. Adapters were removed with Cutadapt, and the reads were filtered against the rDNA with Bowtie 2 (Langmead and Salzberg, 2012). The remaining reads were aligned with Bowtie 1.0 (Langmead et al., 2009), first to the mouse genome (mm9), and remaining unaligned reads to the chicken genome (gal5). Peaks were called with the MACS program version 2.1.0 (Zhang et al., 2008), using a *Rag2*$^{-/-}$ pro-B cell input (GSM1145867, GSM1296537) for mouse and no input for chicken. Chicken reads were counted over union chicken peaks using featureCount version 1.5.0 (Liao et al., 2014). Normalization factors for the scaling of the mouse Pax5 ChIP-seq track based on the chicken spike-in reads were calculated using the estimateSizeFactors function of DESeq2 (Love et al., 2014) with R version 3.4.1 (https://www.r-project.org). This resulted in the following factors: 0.83 (GSM4473547), 2.18 (GSM4473548), 0.78 (GSM4473549), and 0.78 (GSM4473550). Aligned mouse reads were converted to read coverage tracks using a pipeline that involves samtools version 1.9 (Li et al., 2009), bedtools version 2.7.21 (Quinlan and Hall, 2010), and University of California Santa Cruz kent tools (Kuhn et al., 2013), considering the appropriate normalization factors. The aligned chicken reads were deduplicated using the rmdup command (samtools version 1.9) before coverage conversion. Genome-wide read coverages were normalized to the number of aligned reads per million. Peak overlaps were calculated with the Multovl program (Aszódi, 2012). Peak-to-gene assignment was performed as described (Revilla-I-Domingo et al., 2012). Read density profiles were calculated with customized R scripts based on genome-wide peak-centered read coverages.

RNA-seq data processing

Mouse reads that passed the basic quality control (Illumina chastity) were further processed. The first six nucleotides at the

5′ end were trimmed, adapters were removed with Cutadapt, and the reads were filtered against the rDNA with Bowtie 2 (Langmead and Salzberg, 2012). The remaining reads were aligned with TopHat version 1.4.1 (Trapnell et al., 2009) to the transcriptome and full genome of *Mus musculus*, version mm9. Reads were counted over merged gene models using featureCounts version 1.5.0 (Liao et al., 2014). Differential expression between $Igh^{Pax5/+}$ (KI) and $Igh^{+/+}$ (WT) samples were analyzed for each cell type by DESeq2 (Love et al., 2014). In brief, the model design "~ group" and Negative Binomial GLM fitting and Wald statistic ("DESeq" function) were used, whereby "group" specifies the combinations of the conditions (plasma_cell, plasma_blast, wt, ki). Genes with an adjusted P value of <0.05, a mean TPM of >5, and an absolute fold-change of >3 in plasma cells or >2 in plasmablasts, respectively, were called as significantly differentially expressed. Immunoglobulin and TCR genes were filtered from the list of significantly expressed genes. Regularized log transformations were computed with the blind option set to "FALSE" and were transformed from the $\log_2$ to $\log_{10}$ scale for the scatterplots shown in Fig. 4 A and Fig. S3 B. TPM values were calculated as described (Wagner et al., 2012).

GSEA

GSEA was performed using the GSEA software from the Broad Institute (Subramanian et al., 2005). Genes were ranked based on $\log_2$ fold change from the DESeq2 package and compared with our own defined gene sets.

Statistical analysis

Statistical significance was determined with the GraphPad Prism 7 software, using the tests described in each figure legend.

Data availability

The ChIP-seq and RNA-seq data reported in this study (Table S3) are available in GEO under accession no. GSE148556.

Online supplemental material

Fig. S1 shows a schematic diagram of the Igh^{Pax5} allele and the Pax5 protein expression during LPS-induced differentiation of $Igh^{Pax5/+}$ and $Igh^{+/+}$ plasmablasts. Fig. S2 describes the flow-cytometric sorting of LPS-induced $Igh^{Pax5/+}$ and $Igh^{+/+}$ plasmablasts and the Pax5-binding patterns in sorted activated B cells and plasmablasts of both genotypes. Fig. S3 further examines the Pax5-dependent gene expression in $Igh^{Pax5/+}$ plasmablasts and plasma cells. Fig. S4 shows the antibody titers and ER morphology of plasma cells in $Igh^{Pax5/+}$ and $Igh^{+/+}$ mice. Fig. S5 describes the immune responses to SRBC immunization in $Igh^{Pax5/+}$ mice. Table S1 and Table S2 contain the RNA-seq data of all Pax5-regulated genes identified in LPS-induced plasmablasts and ex vivo sorted bone marrow plasma cells of the $Igh^{Pax5/+}$ genotype, respectively. Table S3 describes all Illumina sequencing experiments generated for this study.

Acknowledgments

We thank S. Jurado for help with injection experiments, M. Fischer for initial analysis of RNA-seq data, B. Vilagos for initial immunization experiments, T. Lendl for writing the program script for ELISPOT size analysis, K. Aumayr's team for flow-cytometric sorting, A. Sommer's team at the Vienna BioCenter Core Facilities (VBCF) for Illumina sequencing, and N. Drexler at VBCF for electron microscopy.

This research was supported by Boehringer Ingelheim, the European Research Council under the European Union's Horizon 2020 research and innovation program (grant agreement no. 740349-PlasmaCellControl), the Austrian Industrial Research Promotion Agency (Headquarter Grant FFG-852936), and the Austrian Science Fund (FWF) DK W1212 (to B. Agerer and A. Bergthaler).

Author contributions: G.J. Liu did most experiments; M. Wöhner helped with cell injections and advice on plasma cell experiments; S.G. Malin performed initial plasma cell analyses; M. Jaritz bioinformatically analyzed the RNA-seq and ChIP-seq data; B. Agerer and A. Bergthaler performed immunization experiments; G.J. Liu and M. Busslinger planned the project, designed the experiments, and wrote the manuscript.

Disclosures: The authors declare no competing interests exist.

Submitted: 28 January 2020
Revised: 20 May 2020
Accepted: 1 July 2020

References

Adams, B., P. Dörfler, A. Aguzzi, Z. Kozmik, P. Urbánek, I. Maurer-Fogy, and M. Busslinger. 1992. *Pax-5* encodes the transcription factor BSAP and is expressed in B lymphocytes, the developing CNS, and adult testis. *Genes Dev.* 6:1589–1607. https://doi.org/10.1101/gad.6.9.1589

Alt, F.W., Y. Zhang, F.-L. Meng, C. Guo, and B. Schwer. 2013. Mechanisms of programmed DNA lesions and genomic instability in the immune system. *Cell.* 152:417–429. https://doi.org/10.1016/j.cell.2013.01.007

Aszódi, A.. 2012. MULTOVL: fast multiple overlaps of genomic regions. *Bioinformatics.* 28:3318–3319. https://doi.org/10.1093/bioinformatics/bts607

Barnden, M.J., J. Allison, W.R. Heath, and F.R. Carbone. 1998. Defective TCR expression in transgenic mice constructed using cDNA-based α- and β-chain genes under the control of heterologous regulatory elements. *Immunol. Cell Biol.* 76:34–40. https://doi.org/10.1046/j.1440-1711.1998.00709.x

Bergqvist, P., A. Stensson, N.Y. Lycke, and M. Bemark. 2010. T cell-independent IgA class switch recombination is restricted to the GALT and occurs prior to manifest germinal center formation. *J. Immunol.* 184:3545–3553. https://doi.org/10.4049/jimmunol.0901895

Boller, S., and R. Grosschedl. 2014. The regulatory network of B-cell differentiation: a focused view of early B-cell factor 1 function. *Immunol. Rev.* 261:102–115. https://doi.org/10.1111/imr.12206

Busslinger, M., N. Klix, P. Pfeffer, P.G. Graninger, and Z. Kozmik. 1996. Deregulation of PAX-5 by translocation of the Emu enhancer of the IgH locus adjacent to two alternative PAX-5 promoters in a diffuse large-cell lymphoma. *Proc. Natl. Acad. Sci. USA.* 93:6129–6134. https://doi.org/10.1073/pnas.93.12.6129

Carotta, S., S.N. Willis, J. Hasbold, M. Inouye, S.H. Pang, D. Emslie, A. Light, M. Chopin, W. Shi, H. Wang, et al. 2014. The transcription factors IRF8 and PU.1 negatively regulate plasma cell differentiation. *J. Exp. Med.* 211:2169–2181. https://doi.org/10.1084/jem.20140425

Chevrier, S., C. Genton, A. Kallies, A. Karnowski, L.A. Otten, B. Malissen, M. Malissen, M. Botto, L.M. Corcoran, S.L. Nutt, et al. 2009. CD93 is required for maintenance of antibody secretion and persistence of plasma cells in the bone marrow niche. *Proc. Natl. Acad. Sci. USA.* 106:3895–3900. https://doi.org/10.1073/pnas.0809736106

Chevrier, S., D. Emslie, W. Shi, T. Kratina, C. Wellard, A. Karnowski, E. Erikci, G.K. Smyth, K. Chowdhury, D. Tarlinton, et al. 2014. The BTB-ZF

transcription factor Zbtb20 is driven by Irf4 to promote plasma cell differentiation and longevity. *J. Exp. Med.* 211:827–840. https://doi.org/10.1084/jem.20131831

Cobaleda, C., W. Jochum, and M. Busslinger. 2007. Conversion of mature B cells into T cells by dedifferentiation to uncommitted progenitors. *Nature.* 449:473–477. https://doi.org/10.1038/nature06159

Crotty, S.. 2019. T follicular helper cell biology: a decade of discovery and diseases. *Immunity*. 50:1132–1148. https://doi.org/10.1016/j.immuni.2019.04.011

Delogu, A., A. Schebesta, Q. Sun, K. Aschenbrenner, T. Perlot, and M. Busslinger. 2006. Gene repression by Pax5 in B cells is essential for blood cell homeostasis and is reversed in plasma cells. *Immunity*. 24:269–281. https://doi.org/10.1016/j.immuni.2006.01.012

Fuxa, M., and M. Busslinger. 2007. Reporter gene insertions reveal a strictly B lymphoid-specific expression pattern of *Pax5* in support of its B cell identity function. *J. Immunol.* 178:3031–3037. https://doi.org/10.4049/jimmunol.178.5.3031

Gloury, R., D. Zotos, M. Zuidscherwoude, F. Masson, Y. Liao, J. Hasbold, L.M. Corcoran, P.D. Hodgkin, G.T. Belz, W. Shi, et al. 2016. Dynamic changes in Id3 and E-protein activity orchestrate germinal center and plasma cell development. *J. Exp. Med.* 213:1095–1111. https://doi.org/10.1084/jem.20152003

Gu, H., Y.R. Zou, and K. Rajewsky. 1993. Independent control of immunoglobulin switch recombination at individual switch regions evidenced through Cre-*loxP*-mediated gene targeting. *Cell*. 73:1155–1164. https://doi.org/10.1016/0092-8674(93)90644-6

Gu, Z., M.L. Churchman, K.G. Roberts, I. Moore, X. Zhou, J. Nakitandwe, K. Hagiwara, S. Pelletier, S. Gingras, H. Berns, et al. 2019. *PAX5*-driven subtypes of B-progenitor acute lymphoblastic leukemia. *Nat. Genet.* 51:296–307. https://doi.org/10.1038/s41588-018-0315-5

Hu, B., N. Petela, A. Kurze, K.L. Chan, C. Chapard, and K. Nasmyth. 2015. Biological chromodynamics: a general method for measuring protein occupancy across the genome by calibrating ChIP-seq. *Nucleic Acids Res.* 43. e132.

Ise, W., K. Fujii, K. Shiroguchi, A. Ito, K. Kometani, K. Takeda, E. Kawakami, K. Yamashita, K. Suzuki, T. Okada, et al. 2018. T follicular helper cell-germinal center B cell interaction strength regulates entry into plasma cell or recycling germinal center cell fate. *Immunity*. 48:702–715.e4. https://doi.org/10.1016/j.immuni.2018.03.027

Kallies, A., J. Hasbold, D.M. Tarlinton, W. Dietrich, L.M. Corcoran, P.D. Hodgkin, and S.L. Nutt. 2004. Plasma cell ontogeny defined by quantitative changes in blimp-1 expression. *J. Exp. Med.* 200:967–977. https://doi.org/10.1084/jem.20040973

Kemp, D.J., A. Wilson, A.W. Harris, and K. Shortman. 1980. The immunoglobulin mu constant region gene is expressed in mouse thymocytes. *Nature.* 286:168–170. https://doi.org/10.1038/286168a0

Klein, U., S. Casola, G. Cattoretti, Q. Shen, M. Lia, T. Mo, T. Ludwig, K. Rajewsky, and R. Dalla-Favera. 2006. Transcription factor IRF4 controls plasma cell differentiation and class-switch recombination. *Nat. Immunol.* 7:773–782. https://doi.org/10.1038/ni1357

Kuhn, R.M., D. Haussler, and W.J. Kent. 2013. The UCSC genome browser and associated tools. *Brief. Bioinform.* 14:144–161. https://doi.org/10.1093/bib/bbs038

Kwon, H., D. Thierry-Mieg, J. Thierry-Mieg, H.P. Kim, J. Oh, C. Tunyaplin, S. Carotta, C.E. Donovan, M.L. Goldman, P. Tailor, et al. 2009. Analysis of interleukin-21-induced *Prdm1* gene regulation reveals functional cooperation of STAT3 and IRF4 transcription factors. *Immunity*. 31:941–952. https://doi.org/10.1016/j.immuni.2009.10.008

Langmead, B., and S.L. Salzberg. 2012. Fast gapped-read alignment with Bowtie 2. *Nat. Methods*. 9:357–359. https://doi.org/10.1038/nmeth.1923

Langmead, B., C. Trapnell, M. Pop, and S.L. Salzberg. 2009. Ultrafast and memory-efficient alignment of short DNA sequences to the human genome. *Genome Biol.* 10:R25. https://doi.org/10.1186/gb-2009-10-3-r25

Li, H., B. Handsaker, A. Wysoker, T. Fennell, J. Ruan, N. Homer, G. Marth, G. Abecasis, and R. Durbin; 1000 Genome Project Data Processing Subgroup. 2009. The Sequence Alignment/Map format and SAMtools. *Bioinformatics*. 25:2078–2079. https://doi.org/10.1093/bioinformatics/btp352

Li, W., R. Yu, B. Ma, Y. Yang, X. Jiao, Y. Liu, H. Cao, W. Dong, L. Liu, K. Ma, et al. 2015. Core fucosylation of IgG B cell receptor is required for antigen recognition and antibody production. *J. Immunol.* 194:2596–2606. https://doi.org/10.4049/jimmunol.1402678

Liao, Y., G.K. Smyth, and W. Shi. 2014. featureCounts: an efficient general purpose program for assigning sequence reads to genomic features. *Bioinformatics*. 30:923–930. https://doi.org/10.1093/bioinformatics/btt656

Lin, K.-I., C. Angelin-Duclos, T.C. Kuo, and K. Calame. 2002. Blimp-1-dependent repression of *Pax-5* is required for differentiation of B cells to immunoglobulin M-secreting plasma cells. *Mol. Cell. Biol.* 22:4771–4780. https://doi.org/10.1128/MCB.22.13.4771-4780.2002

Love, M.I., W. Huber, and S. Anders. 2014. Moderated estimation of fold change and dispersion for RNA-seq data with DESeq2. *Genome Biol.* 15:550. https://doi.org/10.1186/s13059-014-0550-8

Medvedovic, J., A. Ebert, H. Tagoh, and M. Busslinger. 2011. Pax5: a master regulator of B cell development and leukemogenesis. *Adv. Immunol.* 111:179–206. https://doi.org/10.1016/B978-0-12-385991-4.00005-2

Medvedovic, J., A. Ebert, H. Tagoh, I.M. Tamir, T.A. Schwickert, M. Novatchkova, Q. Sun, P.J. Huis In 't Veld, C. Guo, H.S. Yoon, et al. 2013. Flexible long-range loops in the V_H gene region of the *Igh* locus facilitate the generation of a diverse antibody repertoire. *Immunity*. 39:229–244. https://doi.org/10.1016/j.immuni.2013.08.011

Minnich, M., H. Tagoh, P. Bönelt, E. Axelsson, M. Fischer, B. Cebolla, A. Tarakhovsky, S.L. Nutt, M. Jaritz, and M. Busslinger. 2016. Multifunctional role of the transcription factor Blimp-1 in coordinating plasma cell differentiation. *Nat. Immunol.* 17:331–343. https://doi.org/10.1038/ni.3349

Nera, K.-P., P. Kohonen, E. Narvi, A. Peippo, L. Mustonen, P. Terho, K. Koskela, J.-M. Buerstedde, and O. Lassila. 2006. Loss of Pax5 promotes plasma cell differentiation. *Immunity*. 24:283–293. https://doi.org/10.1016/j.immuni.2006.02.003

Nutt, S.L., B. Heavey, A.G. Rolink, and M. Busslinger. 1999. Commitment to the B-lymphoid lineage depends on the transcription factor Pax5. *Nature*. 401:556–562. https://doi.org/10.1038/44076

Nutt, S.L., P.D. Hodgkin, D.M. Tarlinton, and L.M. Corcoran. 2015. The generation of antibody-secreting plasma cells. *Nat. Rev. Immunol.* 15:160–171. https://doi.org/10.1038/nri3795

Ochiai, K., Y. Katoh, T. Ikura, Y. Hoshikawa, T. Noda, H. Karasuyama, S. Tashiro, A. Muto, and K. Igarashi. 2006. Plasmacytic transcription factor Blimp-1 is repressed by Bach2 in B cells. *J. Biol. Chem.* 281:38226–38234. https://doi.org/10.1074/jbc.M607592200

Parkhomchuk, D., T. Borodina, V. Amstislavskiy, M. Banaru, L. Hallen, S. Krobitsch, H. Lehrach, and A. Soldatov. 2009. Transcriptome analysis by strand-specific sequencing of complementary DNA. *Nucleic Acids Res.* 37. e123. https://doi.org/10.1093/nar/gkp596

Peperzak, V., I. Vikström, J. Walker, S.P. Glaser, M. LePage, C.M. Coquery, L.D. Erickson, K. Fairfax, F. Mackay, A. Strasser, et al. 2013. Mcl-1 is essential for the survival of plasma cells. *Nat. Immunol.* 14:290–297. https://doi.org/10.1038/ni.2527

Quinlan, A.R., and I.M. Hall. 2010. BEDTools: a flexible suite of utilities for comparing genomic features. *Bioinformatics*. 26:841–842. https://doi.org/10.1093/bioinformatics/btq033

Reimold, A.M., N.N. Iwakoshi, J. Manis, P. Vallabhajosyula, E. Szomolanyi-Tsuda, E.M. Gravallese, D. Friend, M.J. Grusby, F. Alt, and L.H. Glimcher. 2001. Plasma cell differentiation requires the transcription factor XBP-1. *Nature*. 412:300–307. https://doi.org/10.1038/35085509

Revilla-I-Domingo, R., I. Bilic, B. Vilagos, H. Tagoh, A. Ebert, I.M. Tamir, L. Smeenk, J. Trupke, A. Sommer, M. Jaritz, et al. 2012. The B-cell identity factor Pax5 regulates distinct transcriptional programmes in early and late B lymphopoiesis. *EMBO J.* 31:3130–3146. https://doi.org/10.1038/emboj.2012.155

Rodríguez, C.I., F. Buchholz, J. Galloway, R. Sequerra, J. Kasper, R. Ayala, A.F. Stewart, and S.M. Dymecki. 2000. High-efficiency deleter mice show that FLPe is an alternative to Cre-*loxP*. *Nat. Genet.* 25:139–140. https://doi.org/10.1038/75973

Roy, K., S. Mitchell, Y. Liu, S. Ohta, Y.S. Lin, M.O. Metzig, S.L. Nutt, and A. Hoffmann. 2019. A regulatory circuit controlling the dynamics of NFkappaB cRel transitions B cells from proliferation to plasma cell differentiation. *Immunity*. 50:616–628.e6. https://doi.org/10.1016/j.immuni.2019.02.004

Schebesta, A., S. McManus, G. Salvagiotto, A. Delogu, G.A. Busslinger, and M. Busslinger. 2007. Transcription factor Pax5 activates the chromatin of key genes involved in B cell signaling, adhesion, migration, and immune function. *Immunity*. 27:49–63. https://doi.org/10.1016/j.immuni.2007.05.019

Sciammas, R., A.L. Shaffer, J.H. Schatz, H. Zhao, L.M. Staudt, and H. Singh. 2006. Graded expression of interferon regulatory factor-4 coordinates isotype switching with plasma cell differentiation. *Immunity*. 25:225–236. https://doi.org/10.1016/j.immuni.2006.07.009

Shaffer, A.L., M. Shapiro-Shelef, N.N. Iwakoshi, A.-H. Lee, S.-B. Qian, H. Zhao, X. Yu, L. Yang, B.K. Tan, A. Rosenwald, et al. 2004. XBP1, downstream of Blimp-1, expands the secretory apparatus and other

organelles, and increases protein synthesis in plasma cell differentiation. *Immunity*. 21:81–93. https://doi.org/10.1016/j.immuni.2004.06.010

Shi, W., Y. Liao, S.N. Willis, N. Taubenheim, M. Inouye, D.M. Tarlinton, G.K. Smyth, P.D. Hodgkin, S.L. Nutt, and L.M. Corcoran. 2015. Transcriptional profiling of mouse B cell terminal differentiation defines a signature for antibody-secreting plasma cells. *Nat. Immunol*. 16:663–673. https://doi.org/10.1038/ni.3154

Shih, T.-A.Y., M. Roederer, and M.C. Nussenzweig. 2002. Role of antigen receptor affinity in T cell-independent antibody responses in vivo. *Nat. Immunol*. 3:399–406. https://doi.org/10.1038/ni776

Shinkai, Y., G. Rathbun, K.-P. Lam, E.M. Oltz, V. Stewart, M. Mendelsohn, J. Charron, M. Datta, F. Young, A.M. Stall, et al. 1992. RAG-2-deficient mice lack mature lymphocytes owing to inability to initiate V(D)J rearrangement. *Cell*. 68:855–867. https://doi.org/10.1016/0092-8674(92)90029-C

Smith, K.G., A. Light, G.J. Nossal, and D.M. Tarlinton. 1997. The extent of affinity maturation differs between the memory and antibody-forming cell compartments in the primary immune response. *EMBO J*. 16:2996–3006. https://doi.org/10.1093/emboj/16.11.2996

Souabni, A., W. Jochum, and M. Busslinger. 2007. Oncogenic role of Pax5 in the T-lymphoid lineage upon ectopic expression from the immunoglobulin heavy-chain locus. *Blood*. 109:281–289. https://doi.org/10.1182/blood-2006-03-009670

Subramanian, A., P. Tamayo, V.K. Mootha, S. Mukherjee, B.L. Ebert, M.A. Gillette, A. Paulovich, S.L. Pomeroy, T.R. Golub, E.S. Lander, et al. 2005. Gene set enrichment analysis: a knowledge-based approach for interpreting genome-wide expression profiles. *Proc. Natl. Acad. Sci. USA*. 102:15545–15550. https://doi.org/10.1073/pnas.0506580102

Taubenheim, N., D.M. Tarlinton, S. Crawford, L.M. Corcoran, P.D. Hodgkin, and S.L. Nutt. 2012. High rate of antibody secretion is not integral to plasma cell differentiation as revealed by XBP-1 deficiency. *J. Immunol*. 189:3328–3338. https://doi.org/10.4049/jimmunol.1201042

Tellier, J., W. Shi, M. Minnich, Y. Liao, S. Crawford, G.K. Smyth, A. Kallies, M. Busslinger, and S.L. Nutt. 2016. Blimp-1 controls plasma cell function through the regulation of immunoglobulin secretion and the unfolded protein response. *Nat. Immunol*. 17:323–330. https://doi.org/10.1038/ni.3348

Trapnell, C., L. Pachter, and S.L. Salzberg. 2009. TopHat: discovering splice junctions with RNA-Seq. *Bioinformatics*. 25:1105–1111. https://doi.org/10.1093/bioinformatics/btp120

Usui, T., Y. Wakatsuki, Y. Matsunaga, S. Kaneko, H. Koseki, and T. Kita. 1997. Overexpression of B cell-specific activator protein (BSAP/Pax-5) in a late B cell is sufficient to suppress differentiation to an Ig high producer cell with plasma cell phenotype. *J. Immunol*. 158:3197–3204.

Victora, G.D., and M.C. Nussenzweig. 2012. Germinal centers. *Annu. Rev. Immunol*. 30:429–457. https://doi.org/10.1146/annurev-immunol-020711-075032

Wagner, G.P., K. Kin, and V.J. Lynch. 2012. Measurement of mRNA abundance using RNA-seq data: RPKM measure is inconsistent among samples. *Theory Biosci*. 131:281–285. https://doi.org/10.1007/s12064-012-0162-3

Willis, S.N., J. Tellier, Y. Liao, S. Trezise, A. Light, K. O'Donnell, L.A. Garrett-Sinha, W. Shi, D.M. Tarlinton, and S.L. Nutt. 2017. Environmental sensing by mature B cells is controlled by the transcription factors PU.1 and SpiB. *Nat. Commun*. 8:1426. https://doi.org/10.1038/s41467-017-01605-1

Wöhner, M., H. Tagoh, I. Bilic, M. Jaritz, D.K. Poliakova, M. Fischer, and M. Busslinger. 2016. Molecular functions of the transcription factors E2A and E2-2 in controlling germinal center B cell and plasma cell development. *J. Exp. Med*. 213:1201–1221. https://doi.org/10.1084/jem.20152002

Yates, A., W. Akanni, M.R. Amode, D. Barrell, K. Billis, D. Carvalho-Silva, C. Cummins, P. Clapham, S. Fitzgerald, L. Gil, et al. 2016. Ensembl 2016. *Nucleic Acids Res*. 44(D1):D710–D716. https://doi.org/10.1093/nar/gkv1157

Zhang, Y., T. Liu, C.A. Meyer, J. Eeckhoute, D.S. Johnson, B.E. Bernstein, C. Nusbaum, R.M. Myers, M. Brown, W. Li, et al. 2008. Model-based analysis of ChIP-Seq (MACS). *Genome Biol*. 9:R137. https://doi.org/10.1186/gb-2008-9-9-r137

Supplemental material

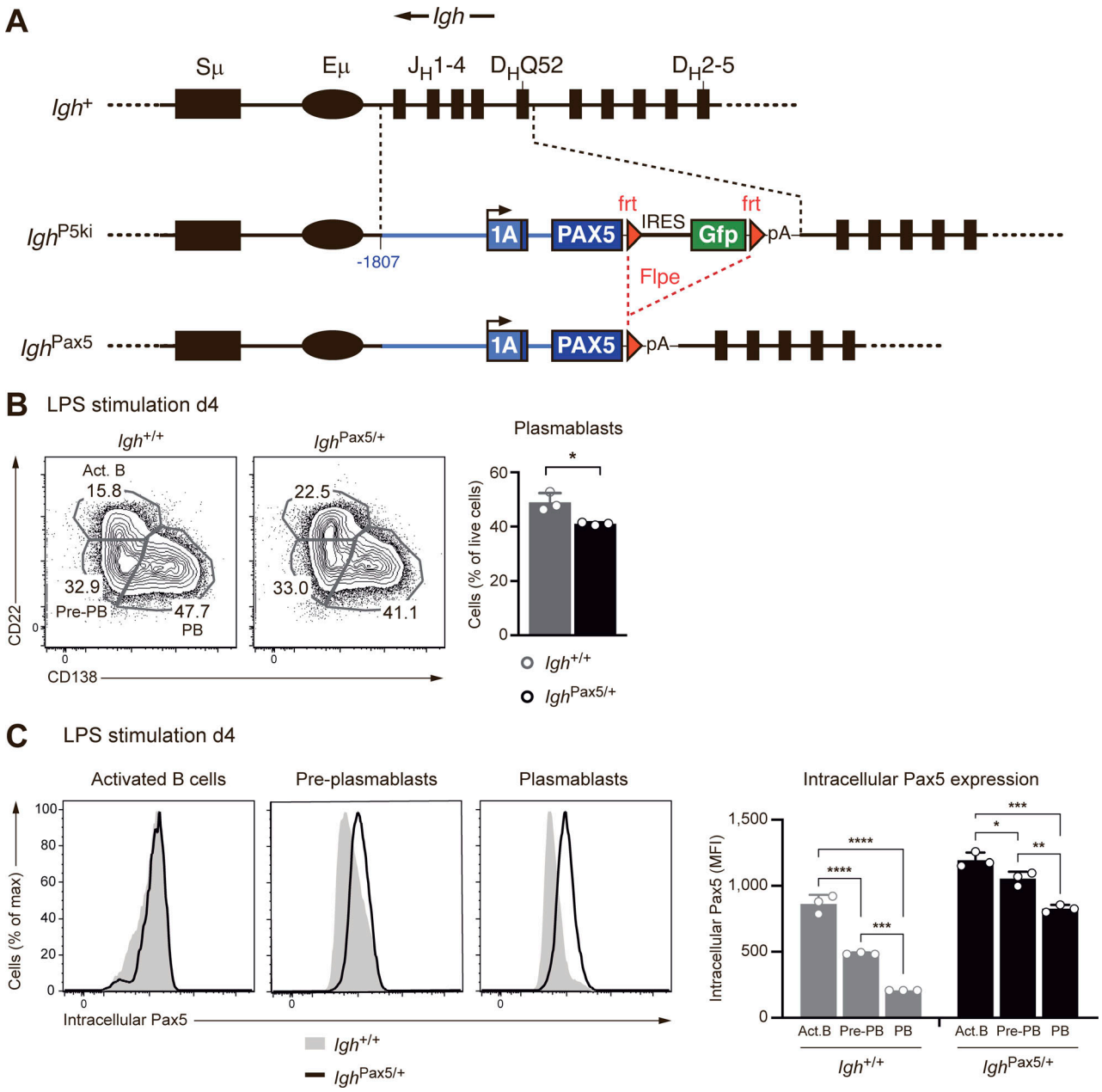

Figure S1. **Schematic diagram and expression of the *Igh*^{Pax5} allele during plasmablast differentiation. (A)** The *Igh*^{P5ki} allele was previously generated by replacing the *Igh* sequences from the J_H1 to the DQ_{52} element with a human *PAX5* minigene that was linked via an internal ribosomal entry sequence (IRES) to a *Gfp* gene (Souabni et al., 2007). The *PAX5* minigene consisted of 1,807 bp of 5′ flanking sequences, the entire exon 1A, a shortened intron 1, and exon 2 fused in frame to *PAX5* cDNA containing exons 3–10. The IRES-Gfp gene, which was flanked by frt sites (red arrowheads), was deleted by Flpe-mediated recombination to generate the *Igh*^{Pax5} allele. pA, polyadenylation site. **(B)** Flow-cytometric analysis and frequencies of activated B cells ($CD22^+CD138^-$), pre-plasmablasts ($CD22^-CD138^-$), and plasmablasts ($CD22^-CD138^+$) at day 4 after LPS stimulation of naive B cells isolated from *Igh*$^{Pax5/+}$ (black) and *Igh*$^{+/+}$ (gray) mice. The percentage of cells in each gate is indicated. The use of CD22 as a surface marker for the definition of pre-plasmablasts and plasmablasts was previously described (Minnich et al., 2016). **(C)** Flow-cytometric analysis of Pax5 expression by intracellular staining of the activated B cells (Act. B), pre-plasmablasts (pre-PB), and plasmablasts (PB) shown in B. The mean fluorescence intensity (MFI) of Pax5 staining is quantified for the indicated cell types of the *Igh*$^{+/+}$ (gray) and *Igh*$^{Pax5/+}$ (black) genotypes (right). Statistical data are shown as mean values with SD and were analyzed by one-way ANOVA followed by Tukey's multiple comparison test; *, $P < 0.05$; **, $P < 0.01$; ***, $P < 0.001$; ****, $P < 0.0001$. Each dot corresponds to one mouse.

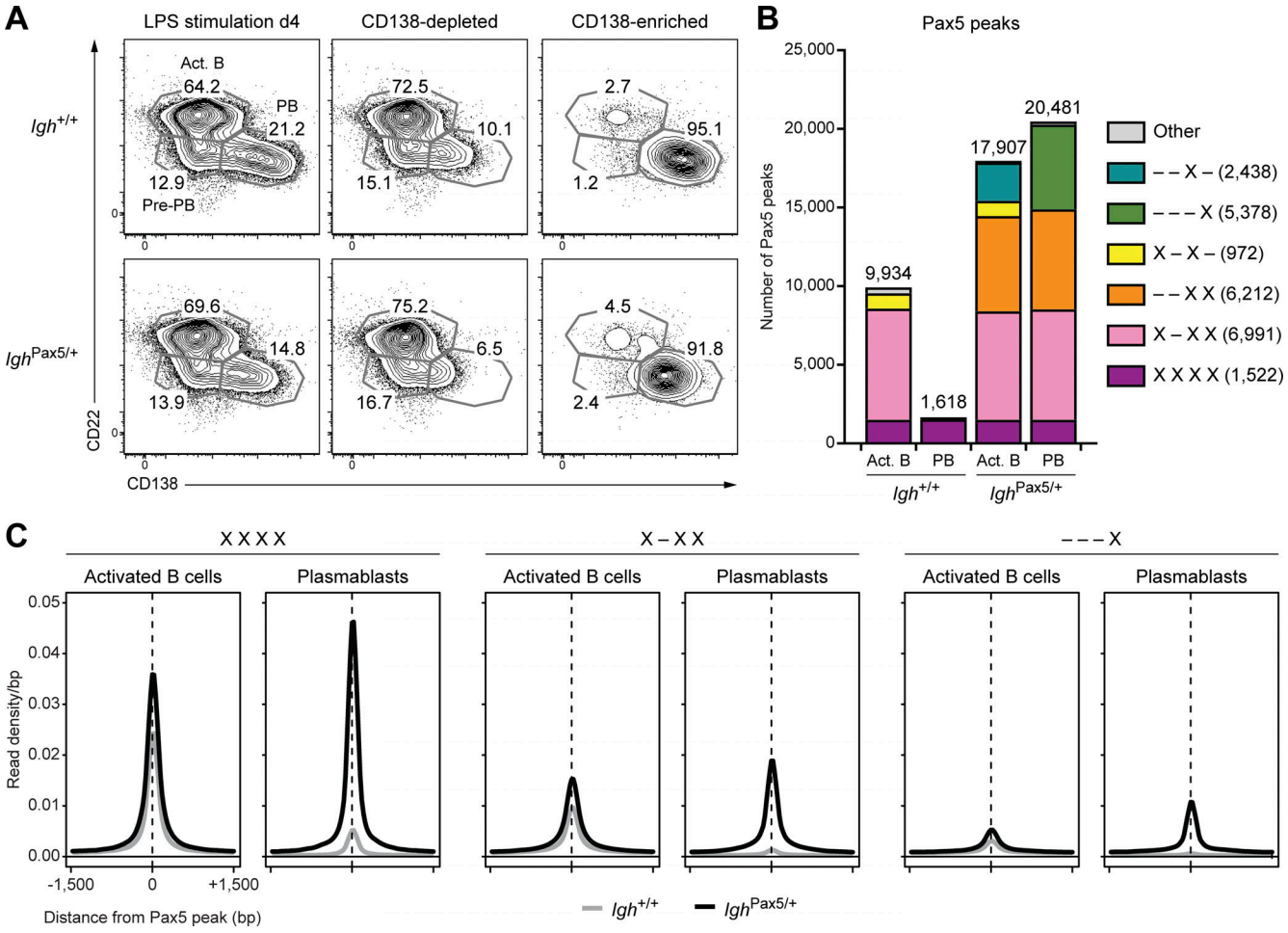

Figure S2. **Pax5-binding patterns in sorted activated B cells and plasmablasts. (A)** CD43⁻ B cells from the spleen of $Igh^{Pax5/+}$ and $Igh^{+/+}$ mice were stimulated with LPS for 4 d before immunomagnetic enrichment of plasmablasts ($CD22^{-}CD138^{+}$) with CD138-MicroBeads to a purity of 92–95%. The CD138-depleted cell fractions, which were strongly enriched for activated B cells (73–75%), were subsequently referred to as "activated B cells." **(B)** The indicated numbers of Pax5 peaks, determined by ChIP-seq analysis in activated B cells and plasmablasts of the $Igh^{Pax5/+}$ or $Igh^{+/+}$ genotype (Fig. 3 A), were identified by stringent MACS peak calling with a P value of $<10^{-10}$. Comparison of the presence of each Pax5 peak in the different cell types identified six major distinct binding categories (indicated by different colors) that are abbreviated by the presence (X) or absence (–) of the same Pax5 peak in each cell type. The number of Pax5 peaks in each category is indicated in brackets to the right. **(C)** Densities of Pax5 binding in the three indicated categories. Average read density profiles aligned at the center of the Pax5 peak are shown for activated B cells (left) and plasmablasts (right) of the $Igh^{Pax5/+}$ (black line) or $Igh^{+/+}$ (gray line) genotype.

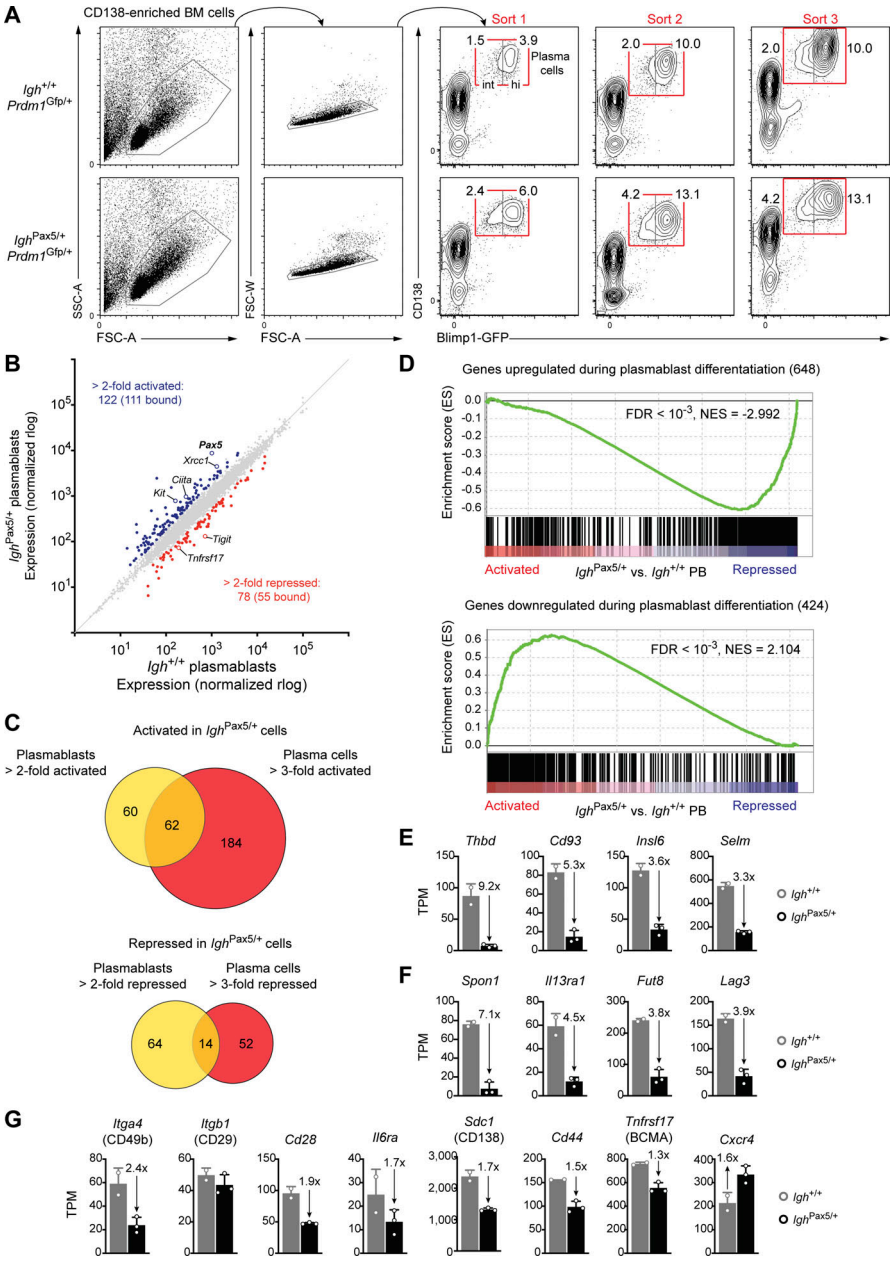

Figure S3. **Pax5-dependent gene expression in $Igh^{Pax5/+}$ plasmablasts and plasma cells. (A)** Flow-cytometric sorting of bone marrow plasma cells used for RNA-seq. Bone marrow cells from 6–8-mo-old $Igh^{+/+}$ $Prdm1^{Gfp/+}$ or $Igh^{Pax5/+}$ $Prdm1^{Gfp/+}$ mice were enriched for CD138$^+$ cells by immunomagnetic selection with CD138-MicroBeads before flow-cytometric sorting of CD138$^+$GFP$^+$ plasma cells. The sorting gate is shown in red for three different sorting experiments. The percentages of GFP^{int} and GFP^{hi} cells in the plasma cell gate are indicated. **(B)** Scatter plot of gene expression differences between $Igh^{Pax5/+}$ and $Igh^{+/+}$ plasmablasts that were sorted as CD22$^-$CD138$^+$GFP$^+$ cells after 4 d of LPS stimulation. The expression data of individual genes (indicated by dots) are plotted as normalized rlog (regularized logarithm) values. Genes with an expression difference of greater than twofold, an adjusted P value of <0.05, and a TPM value of >5 (in at least one sample) are colored in blue or red, corresponding to activation or repression by Pax5. The reference gene *Pax5* (in bold) and five genes previously identified as activated or repressed Pax5 target genes in pro-B or mature B cells (Revilla-I-Domingo et al., 2012) are highlighted by open circles. **(C)** Overlap of Pax5-activated (top) or Pax5-repressed (bottom) genes between $Igh^{Pax5/+}$ plasmablasts (greater than twofold) and $Igh^{Pax5/+}$ plasma cells (greater than threefold). The number of genes in each sector of the Venn diagram is indicated. **(D)** GSEA of 648 up-regulated (top) or 424 down-regulated (bottom) genes in plasmablasts, as compared with the ranked $\log_2$-fold expression changes in $Igh^{Pax5/+}$ versus $Igh^{+/+}$ plasmablasts (PB). The 648 and 424 genes were previously identified as being up-regulated or down-regulated greater than threefold in LPS-generated plasmablasts compared with activated B cells, respectively (Minnich et al., 2016). NES, normalized enrichment score; FDR, false discovery rate. **(E–G)** Expression of selected genes in $Igh^{Pax5/+}$ (black) and $Igh^{+/+}$ (gray) plasma cells, analyzed by the RNA-seq experiments shown in Fig. 4 A. The expression data are shown as mean TPM values with SD and are based on two ($Igh^{+/+}$) and three ($Igh^{Pax5/+}$) independent RNA-seq experiments. Each dot represents one experiment performed with pooled plasma cells from 5–10 mice per genotype. **(E)** Pax5-bound and -repressed genes in $Igh^{Pax5/+}$ plasma cells that were previously identified as repressed Pax5 target genes in pro-B cells or mature B cells (Schebesta et al., 2007; Revilla-I-Domingo et al., 2012). **(F)** Pax5-bound and -repressed genes in $Igh^{Pax5/+}$ plasma cells that have not been identified as Pax5-regulated genes in developing B cells. **(G)** Genes coding for cell adhesion molecules and cell surface receptors that play an important role in controlling the homing and survival of long-lived plasma cells in the bone marrow niche. SSC, side scatter; FSC, forward scatter; A, area; W, width.

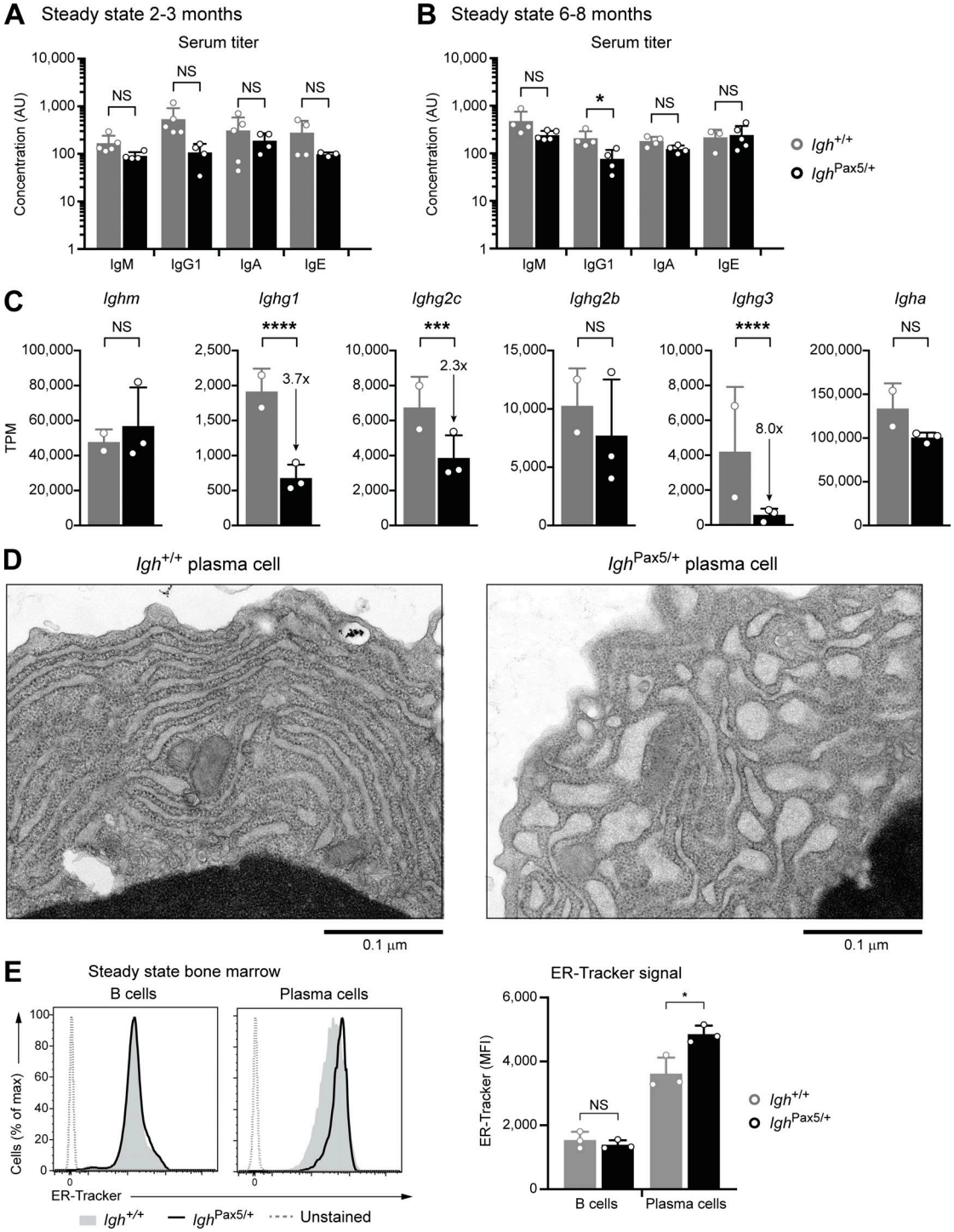

Figure S4. **Antibody titers and morphology of plasma cells in *Igh*$^{Pax5/+}$ mice. (A and B)** Serum titers of total antibody of the IgM, IgG1, IgA, and IgE isotypes in nonimmunized *Igh*$^{Pax5/+}$ (black) and *Igh*$^{+/+}$ (gray) mice at the age of 2–3 mo (A) or 6–8 mo (B). The results shown are representative of three independent experiments. Statistical data (A and B) are shown as mean values with SD and were analyzed by the two-tailed unpaired Student's *t* test; *, P < 0.05. NS, not significant (P > 0.05). **(C)** Expression of the indicated immunoglobulin isotype mRNAs in *Igh*$^{Pax5/+}$ (black) and *Igh*$^{+/+}$ (gray) plasma cells. The expression data are shown as mean TPM values with SD and are based on two (*Igh*$^{+/+}$) and three (*Igh*$^{Pax5/+}$) independent RNA-seq experiments. Each dot represents one experiment performed with pooled plasma cells from 5–10 mice per genotype. The P values were calculated by the DESeq2 program; ***, P < 0.001; ****, P < 0.0001. NS, not significant (P > 0.05). **(D)** Higher magnification of the same two electron microscope images shown in Fig. 5 E. The two plasma cells were isolated from the bone marrow of 6–8-mo-old *Igh*$^{Pax5/+}$ and *Igh*$^{+/+}$ mice. **(E)** Comparison of ER content in B cells and plasma cells. Staining with the ER-Tracker Red dye (at a final concentration of 0.2 μM) was used to determine the ER content of B cells (CD19$^+$) and plasma cells (Blimp1-GFP$^+$CD138$^+$) in the bone marrow of 6–8-mo-old *Igh*$^{Pax5/+}$ and *Igh*$^{+/+}$ mice at steady state (left). The quantification of the staining is shown as mean fluorescence intensity (MFI; right). Statistical data (A, B, and E) are shown as mean values with SD and were analyzed by the two-tailed unpaired Student's *t* test; *, P < 0.05. NS, not significant (P > 0.05). Each dot (A, B, and E) corresponds to one mouse.

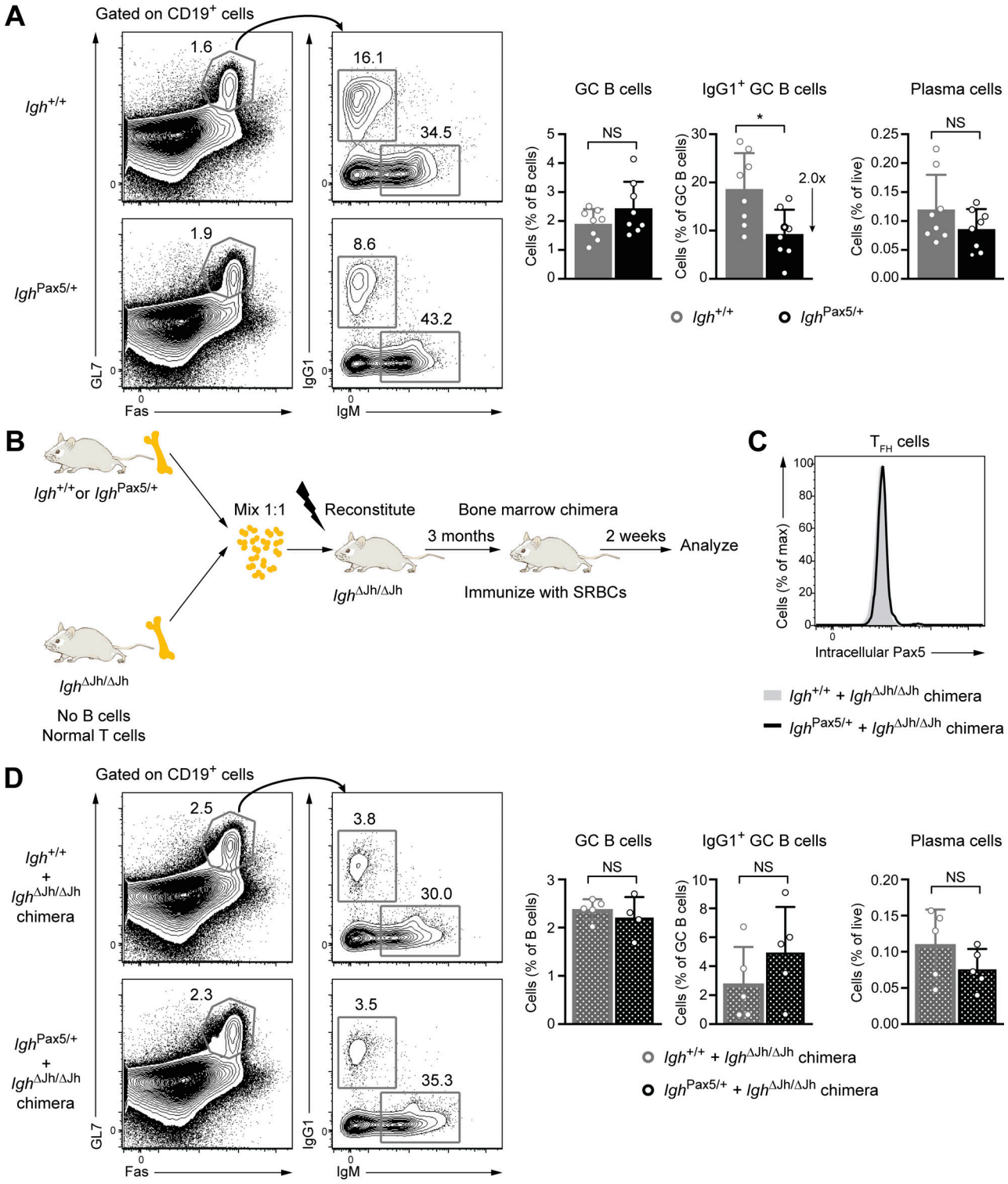

Figure S5. **Immune responses to SRBC immunization in *Igh*$^{Pax5/+}$ mice. (A)** GC B cell response in the spleen of *Igh*$^{+/+}$ and *Igh*$^{Pax5/+}$ mice 14 d after immunization with SRBCs. Total GC B cells (CD19$^+$GL7$^+$Fas$^+$) and IgG1$^+$ GC B cells were analyzed by flow cytometry (left), and their frequency was quantified (right) together with the frequency of splenic plasma cells (Lin$^-$B220^{int}CD138$^+$Blimp1-GFP$^+$). The data are pooled from two independent experiments. **(B)** Schematic diagram describing the generation of mixed bone marrow chimeras. Lineage-depleted bone marrow cells from *Igh*$^{Pax5/+}$ or control *Igh*$^{+/+}$ mice were mixed at a 1:1 ratio with lineage-depleted bone marrow cells from J_HT mice before injection into lethally irradiated J_HT recipient mice. 3 mo after reconstitution, the bone marrow chimeric mice were immunized with SRBCs and analyzed 2 wk later. **(C)** Flow-cytometric analysis of intracellular Pax5 protein levels in T_{FH} cells (CD4$^+$CXCR5$^+$PD1$^+$Bcl6$^+$) from the spleen of chimeric mice reconstituted with J_HT and *Igh*$^{Pax5/+}$ (black line) or *Igh*$^{+/+}$ (gray filled) bone marrow cells. **(D)** Flow-cytometric analysis of the GC B cell response (left) and frequency of the indicated cell types (right) in the spleen of chimeric mice 2 wk after immunization with SRBCs. The data shown are representative of two independent experiments. Statistical data (A and D) are shown as mean values with SD and were analyzed by the two-tailed unpaired Student's *t* test; *, P < 0.05. NS, not significant (P > 0.05). Each dot corresponds to one mouse.

Tables S1–S3 are provided online as separate Excel files. Table S1 shows Pax5-activated genes determined by RNA-seq of LPS-generated $Igh^{+/+}$ (WT) and $Igh^{Pax5/+}$ (KI) plasmablasts. Table S2 shows Pax5-activated genes determined by RNA-seq of ex vivo sorted $Igh^{+/+}$ (WT) and $Igh^{Pax5/+}$ (KI) bone marrow plasma cells. Table S3 describes all Illumina sequencing experiments generated for this study (GSE148556).